Contents lists available at ScienceDirect

Journal of Fluids and Structures

journal homepage: www.elsevier.com/locate/jfs



Wave-induced reconfiguration of and drag on marsh plants



Xiaoxia Zhang a,b,*, Heidi Nepfa

- ^a Department of Civil and Environmental Engineering, Massachusetts Institute of Technology, USA
- ^b State Key Laboratory of Hydraulics and Mountain River Engineering, Sichuan University, China

ARTICLE INFO

Article history: Received 26 April 2020 Received in revised form 16 September 2020 Accepted 12 November 2020 Available online xxxx

Keywords: Salt marsh Flexible plant Reconfiguration Drag force

ABSTRACT

Salt marshes are a common feature in coastal regions and have been noted for their ability to attenuate wave energy, providing an important first line of coastal defense. Marsh plants usually consist of multiple leaves distributed along a central stem. This paper constructed a model predicting wave force on a marsh plant by modeling the reconfiguration of both the leaves and stem in waves. The individual leaf and stem models and the full plant model were validated with experimental measurements of drag and plant motion using both live and dynamically-similar model plants under a range of wave conditions. Although the leaves exhibited greater reconfiguration than the stem, they contributed more than 70% of the plant drag. Plant reconfiguration produced a drag force that had a weaker than quadratic dependence on wave velocity. A simplified model, which combines scaling laws for the stem and individual leaves, is proposed and validated. Wave drag on a variety of marsh species with different morphology and rigidity were estimated and compared.

© 2020 Elsevier Ltd. All rights reserved.

1. Introduction

Salt marshes are widely distributed in the upper intertidal zone around the world. They provide food and refuge for fish and invertebrates (Boesch and Turner, 1984), produce and store blue carbon (Mcleod et al., 2011), and protect the coasts and coastal communities from erosion, storm surge, and small tsunami waves (Gedan et al., 2011). Because salt marshes provide these important ecosystem services, the protection and restoration of this green infrastructure (also known as nature-based solutions) have become a focal point in coastal management (e.g. Sutton-Grier et al., 2015). In particular, nature-based solutions involve the engineering and management of vegetated habitats as a first line of defense against coastal flooding. A key component of this defense is the attenuation of waves. The motivation for this study is to provide a predictive model for the drag on realistic marsh plants, which can be the foundation for predicting wave attenuation. While many field observations have documented the ability of particular marshes to mitigate storm waves and surges (e.g. Moeller et al., 1996; Yang et al., 2012; Ysebaert et al., 2011), the prediction of storm mitigation by marshes is currently limited by the inability to predict the hydrodynamic drag provided by marsh plants, which have a complex and flexible morphology. This study examined the impact of both morphology (leaves and stem) and flexibility on the hydrodynamic drag imparted by marsh plants, which provides the basis for predicting wave attenuation.

Salt marsh plants, such as *Phragmites australis* (Common Reed), *Scirpus maritimus* (also called *Bolboschoenus maritimus*), *Spartina alterniflora* (smooth cordgrass), *Spartina cynosuroides* (Big Cordgrass), and *Spartina Patens* (Salt Hay Grass), are composed of multiple long flexible leaves attached to a comparatively more rigid stem. Because the leaves reconfigure

^{*} Corresponding author at: State Key Laboratory of Hydraulics and Mountain River Engineering, Sichuan University, China. E-mail address: xiaoxia@mit.edu (X. Zhang).

(bend) more easily in waves, their fractional contribution to the total plant drag is expected to decrease with increasing wave intensity. A similar shift in leaf contribution has been observed in other plants under unidirectional flow. For example, Jalonen and Järvelä (2013) showed that leaves contributed up to 80% of the total drag when sample trees were towed in a water tank at low velocity (0.1 m/s), but only 40% when velocity exceeded 0.8 m/s.

Currently, there is no theoretical model that describes the dynamic reconfiguration of and drag on a marsh plant. Previous studies have empirically quantified drag and wave attenuation using laboratory experiments with model plants (e.g. Anderson and Smith, 2014; Koftis et al., 2013) and live plants (e.g. Wang et al., 2016) and through field surveys (e.g. Cooper, 2005; Knutson et al., 1982; Moeller et al., 1996; Rupprecht, 2015; Wayne, 1976; Yang et al., 2012). While many of these studies recognize the role of morphology and reconfiguration on plant drag and wave attenuation, these attributes have not been explicitly modeled. Instead, previous studies have used the stem length and diameter to represent the whole plant and then fit an empirical drag coefficient. These fitted drag coefficients cannot be applied with confidence to other sites, because the drag coefficient depends on plant properties. Consequently, detailed studies considering plant dynamics and the roles of both the leaves and the stem are needed to build a predictive wave-drag model for marsh plants.

A few studies have modeled the dynamics of individual flexible blades (representing seagrass and reeds) as flat plates (Méndez et al., 1999) and cantilever beams (Bradley and Houser, 2009; Mullarney and Henderson, 2010), Luhar and Nepf (2016) considered both the flexibility and buoyancy of flat blades. In their model, the dynamic reconfiguration of a blade is characterized by three dimensionless parameters (Luhar and Nepf, 2016): the Buoyancy number B, which is the ratio of the restoring forces due to buoyancy and stiffness; the wave Cauchy number Ca, which is the ratio of the hydrodynamic drag to the restoring force due to blade stiffness, and the blade length ratio L, which is the ratio of blade length to the wave excursion,

$$B = \frac{\Delta \rho g b d l^3}{E I} \tag{1}$$

$$B = \frac{\Delta \rho g b d l^3}{E I}$$

$$Ca = \frac{\rho b U_w^2 l^3}{E I / l^2}$$

$$L = \frac{l}{A_w} = \frac{l \omega}{U_w}$$
(1)
(2)

$$L = \frac{l}{A_{vv}} = \frac{l\omega}{U_{vv}} \tag{3}$$

Here, $\Delta \rho = \rho - \rho_p$ is the density difference between water (ρ) and plant (ρ_p) . g is the gravitational acceleration. b, d, and l are the width, thickness, and length of the blade, respectively. U_w is the wave orbital velocity. E is the elastic modulus and $I = bd^3/12$ is the second momentum of inertia. $A_w = U_w/\omega$ is the wave excursion (wave orbital radius), and ω is the wave angular frequency.

To describe the effect of blade reconfiguration on blade drag, Luhar and Nepf (2011) proposed an effective blade length, l_e , defined as the length of a rigid vertical blade that generates the same drag as a flexible blade of length l. When the plant density is comparable to the density of water, plant buoyancy does not impact the blade posture significantly, and B can be neglected. Then, for L > 1, l_e/l is a function of Ca and L (Luhar and Nepf, 2016),

$$\frac{l_e}{l} \sim (CaL)^{-1/4} \tag{4}$$

This scaling law has been verified for individual blades (Luhar and Nepf, 2016) and individual blades within a meadow (Luhar et al., 2017). Applying this scaling law, Lei and Nepf (2019) were able to predict the wave decay over a meadow of model seagrass by modifying the classic theoretical prediction for wave damping due to an array of rigid cylinders of height I (Dalrymple et al., 1984). Specifically, Lei and Nepf (2019) adapted this prediction by replacing the rigid plant height with the effective meadow height. These studies showed that models describing drag force on an individual plant can be successfully scaled up to predict the wave damping by a meadow of plants. Seagrass can be represented by an array of individual blades, but marsh plants have a more complex morphology. Each plant has a relatively more rigid stem with multiple flexible leaves distributed along the stem length. This study constructed a model that predicts the reconfiguration of and drag on a marsh plant and tested the prediction against a real specimen of Spartina alterniflora.

2. Theoretical model

This section develops a model to describe the reconfiguration of and drag on a marsh plant comprised of a single stem with evenly distributed leaves (Fig. 1a), such as Spartina alterniflora, Spartina Patens, Spartina cynosuroides, Phragmites australis, and Scirpus maritimus. The following assumptions have been made. (1) The plant is assumed to have N_l leaves distributed both along the stem and around the stem circumference with a constant angle α between each leaf and stem. (2) The density of the plant material is uniform and constant (ρ_p) . (3) Each leaf has the same size (length l_l , width b_l , and thickness d) and elastic modulus E_l . (4) The stem diameter D and elastic modulus E_s are constant. (5) The drag force on the leaves is transmitted to the stem and can be treated as uniformly distributed force on the stem. (6) The force contribution from N_l leaves can be represented by the drag on a representative flat leaf with vertical orientation. Experiments described in Section 3 support these assumptions.

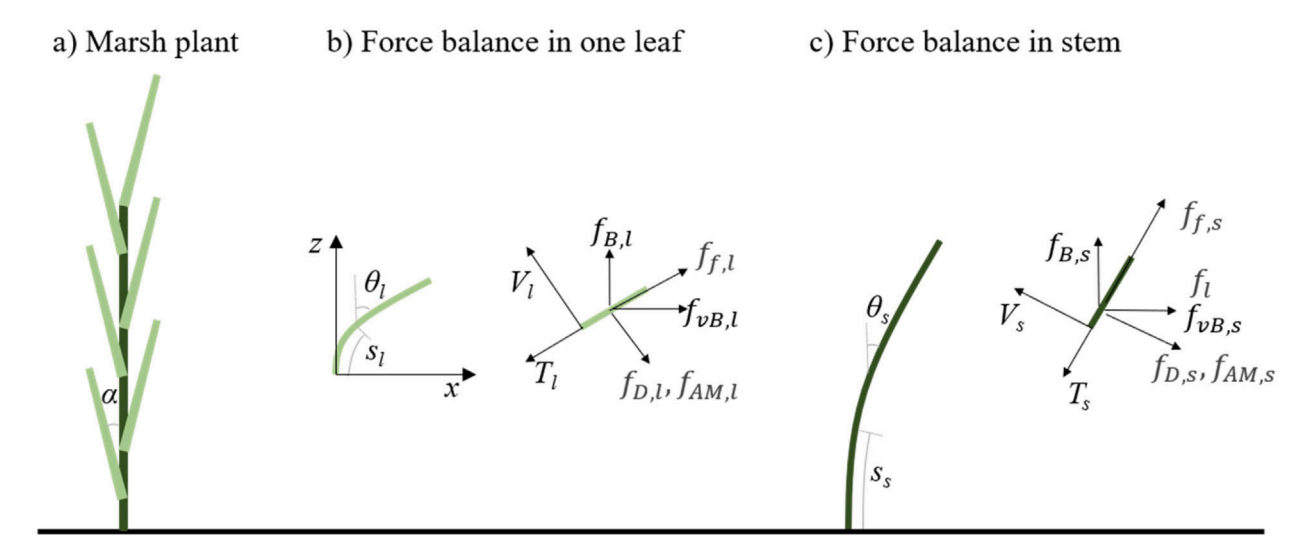


Fig. 1. Schematic showing the coordinate system and forces on the leaf and the stem of a marsh plant, such as Phragmites australis, Scirpus maritimus, Spartina alterniflora, Spartina cynosuroides, and Spartina Patens. Subscript I and s indicate parameters associated with a leaf or a stem, respectively.

We first describe the dynamic reconfiguration of an individual flexible leaf with an initially vertical posture, i.e. the representative leaf, shown in Fig. 1b. Assuming that the leaf is inextensible and moves in a two-dimensional plane (Luhar and Nepf, 2016), i.e. no lateral deflection and only moves in the xz plane, where x and z indicate the wave propagation direction and the vertical direction. The coordinate along the leaf is s_l , with $s_l = 0$ at the base and $s_l = l_l$ at the top of leaf, and l_l is the height of the leaf when fully erect. θ_l is the local angle between the leaf and vertical. Throughout the text the subscript l denotes variables associated with the leaf, and the subscript s denotes variables associated with the stem. The force balance on a single leaf is the same as that for a single blade, as described in Luhar and Nepf (2016), i.e.,

$$\frac{\partial}{\partial s_l}((V_l + iT_l)e^{-i\theta_l}) + if_{B,l} + (f_{D,l} + if_{F,l} + f_{AM,l})e^{-i\theta_l} + f_{VB,l} = \rho_p bd \frac{\partial^2 \tilde{x}}{\partial t^2}$$

$$\tag{5}$$

in which $\tilde{x} = x + iz$ (= $\int_0^{s_l} ie^{-i\theta_l} ds'$, s' is a dummy variable) is the position along the leaf and t is time. $V_l = -\frac{\partial}{\partial s_l} (E_l I_l \frac{\partial \theta_l}{\partial s_l})$ is the restoring force due to leaf rigidity and acts in the leaf-normal direction, $I_l = bd^3/12$ is the second moment of area for the leaf. T_l is the tension in the leaf and acts in the leaf-parallel direction. The external forces and inertia force per unit length in the leaf include: (1) the buoyancy force $f_{B,l} = \Delta \rho gbd$, which acts in the vertical direction; (2) the drag force $f_{D,l} = \frac{1}{2} \rho C_D b \left| \Re(\tilde{u}_R e^{i\theta_l}) \right| \Re(\tilde{u}_R e^{i\theta_l})$, which acts in the leaf-normal direction, C_D is the drag coefficient, $\Re(\tilde{u}_R e^{i\theta_l})$ is the leaf normal component of the relative velocity (\tilde{u}_R) between the fluid (\tilde{u}) and the leaf $(\partial \tilde{x}/\partial t)$, and $\mathfrak{R}()$ denotes the real component; (3) the skin friction $f_{F,l} = \frac{1}{2}\rho C_f b \left|\Im(\tilde{u}_R e^{i\theta_l})\right|\Im(\tilde{u}_R e^{i\theta_l})$, which acts in the leaf-parallel direction, C_f is the skin friction coefficient, $\Im(\tilde{u}_R e^{i\theta_l})$ is the leaf-parallel component of relative velocity, and $\Im()$ denotes the imaginary component; (4) the force due to added mass $f_{AM,l} = \rho k' \frac{\pi b^2}{4} \Re(\frac{\partial \tilde{u}_R}{\partial t} e^{i\theta_l})$, which depends on the relative acceleration between the fluid and the leaf-normal direction, $k' (= C_M - r_A)$ is the added mass coefficient (Keulegan and Carpenter, 1958), C_M is the inertial coefficient and $r_A = bd/(\pi d^2/4) = 4b/\pi d$ is the ratio between the cross-sectional area and the circular area defined by the dimension of the leaf; (5) the Froude-Krylov (or virtual buoyancy) force $f_{VB,l} = \rho b d \frac{\partial \tilde{u}}{\partial t}$, which acts in the direction of flow acceleration; and finally (6) the leaf inertia $\rho_p b d \frac{\partial^2 \hat{x}}{\partial t^2}$, which acts in the direction of leaf acceleration. Eq. (5) can be written in terms of nondimensional variables (denoted with a carat hat), using the following relations:

 $s_l = l_l \hat{s}, t = \hat{t}/\omega, \tilde{u} = \hat{u}U_w, T_l = \hat{T}(E_l I_l/l_l^2), \text{ and } \tilde{x} = l_l \hat{x}, \text{ see details in (Luhar and Nepf, 2016).}$

$$\frac{\partial}{\partial \hat{\mathbf{s}}} \left(-\frac{\partial^{2} \theta_{l}}{\partial \hat{\mathbf{s}}^{2}} + i\hat{T} \right) - i\frac{\partial \theta_{l}}{\partial \hat{\mathbf{s}}} \left(-\frac{\partial^{2} \theta_{l}}{\partial \hat{\mathbf{s}}^{2}} + i\hat{T} \right) + iB_{l}e^{i\theta_{l}} + \frac{1}{2}C_{D}Ca_{l} \left| \Re \left(\hat{u}_{R}e^{i\theta_{l}} \right) \right| \Re(\hat{u}_{R}e^{i\theta_{l}})
+ i\frac{1}{2}C_{f}Ca_{l} \left| \Im \left(\hat{u}_{R}e^{i\theta_{l}} \right) \right| \Im(\hat{u}_{R}e^{i\theta_{l}}) + \frac{2\pi^{2}}{4}k'\frac{Ca_{l}}{KC_{l}}\Re(\frac{\partial \hat{u}_{R}}{\partial \hat{t}}e^{i\theta_{l}})
+ 2\pi\frac{Ca_{l}d/b}{KC_{l}} \left(\frac{\partial \hat{u}}{\partial \hat{t}} - \frac{\rho_{p}}{\rho}L_{l}\frac{\partial^{2}\hat{x}}{\partial \hat{t}^{2}} \right) e^{i\theta_{l}} = 0$$
(6)

The Buoyancy number B_l , Cauchy number Ca_l , and length ratio L_l for the leaf were defined in Eqs. (1), (2), and (3), respectively. KC_l is the Keulegan-Carpenter number (Keulegan and Carpenter, 1958) for the leaves ($KC_l = U_w T_w/b$, T_w is the wave period).

The forces on the leaves are transmitted as a normal $(V_{l0} = -E_l I_l(\frac{\partial^2 \theta_l}{\partial \hat{s}^2}|_{\hat{s}=0}))$ and parallel $(T_{l0} = T_l|_{\hat{s}=0})$ force to the stem at their point of attachment $(s_l = 0, i.e. \, \hat{s} = 0)$. The plant is assumed to have N_l leaves distributed both along the stem and around the stem circumference with a constant angle between leaf and stem α . Experiments discussed below verify that the drag on leaves with an angle to stem can be inferred from the drag on an isolated vertical leaf. With leaves uniformly distributed along the stem, the total force from all leaves can be represented by a distributed force, i.e. a leaf force per unit stem length,

$$f_{l} = \frac{C_{s}N_{l}\left(-V_{l0} - iT_{l0}\right)}{l_{s}} \tag{7}$$

in which $0 \le C_s \le 1$ represents the impact of sheltering and interaction between the leaves and the stem, $C_s = 1$ indicates no sheltering. The value of C_s is determined from experimental measurements reported in the results.

The force balance on the stem at location s_s is similar in form to Eq. (5) (Fig. 1c), but also contains the distributed force, f_i , transmitted from the leaves to the stem,

$$\frac{\partial}{\partial s_s} \left(V_s + i T_s \right) e^{-i\theta_s} + i f_{B,s} + \left(f_{D,s} + i f_{F,s} + i f_{AM,s} \right) e^{-i\theta_s} + f_{VB,s} + f_l = \rho_p \pi (D/2)^2 \frac{\partial^2 \tilde{\chi}}{\partial t^2}$$
(8)

Here, the variables have the same physical meaning as Eq. (5) except the subscript s denotes variables associated with stem. With non-dimensional parameters (denoted with hat notation) $s_s = \hat{s}l_s$, $t = \hat{t}/\omega$, $\tilde{u} = \hat{u}U_w$, $T_s = \hat{T}(E_s l_s/l_s^2)$, and $\tilde{x} = l_s \hat{x}$, Eq. (8) can be written in dimensionless form, i.e.,

$$\frac{\partial}{\partial \hat{s}} \left(-\frac{\partial^{2} \theta_{s}}{\partial \hat{s}^{2}} + i\hat{T} \right) - i\frac{\partial \theta_{s}}{\partial \hat{s}} \left(-\frac{\partial^{2} \theta_{s}}{\partial \hat{s}^{2}} + i\hat{T} \right) + iB_{s}e^{i\theta_{s}} + \frac{C_{s}N_{l}\left(-V_{l0} - iT_{l0} \right)}{E_{s}I_{s}/I_{s}^{2}} e^{i\theta_{s}}
+ \frac{1}{2}C_{D}Ca_{s} \left| \Re\left(\hat{u}_{R}e^{i\theta_{s}}\right) \right| \Re\left(\hat{u}_{R}e^{i\theta_{s}}\right) + i\frac{1}{2}C_{f}Ca_{s} \left| \Im\left(\hat{u}_{R}e^{i\theta_{s}}\right) \right| \Im\left(\hat{u}_{R}e^{i\theta_{s}}\right)
+ \frac{2\pi^{2}}{4}K'\frac{Ca_{s}}{KC_{s}}\Re\left(\frac{\partial \hat{u}_{R}}{\partial \hat{t}}e^{i\theta_{s}}\right) + \frac{2\pi^{2}}{4}\frac{Ca_{s}}{KC_{s}}\left(\frac{\partial \hat{u}}{\partial \hat{t}} - \frac{\rho_{p}}{\rho}L_{s}\frac{\partial^{2} \hat{x}}{\partial \hat{t}^{2}}\right)e^{i\theta_{s}} = 0$$
(9)

in which B_s , Ca_s , and L_s are the Buoyancy number, Cauchy number, and length ratio for the stem. $KC_s = U_w T_w/D$ is the Keulegan–Carpenter number for the stem (Keulegan and Carpenter, 1958).

3. Laboratory experiments

Laboratory experiments were used to confirm the assumptions behind the theoretical model and to validate the model with measurements of drag and motion for both model and live plants. A 1:5 scaled model of the marsh plant *Spartina alterniflora* was constructed based on plant parameters collected at Hangzhou Bay (Zhang et al., 2020) (shown in Fig. 2c). The model plant had one stem and ten leaves. The stem diameter and length were 2 mm and 19 cm, respectively. The leaves were 10-cm long, 3-mm wide, and 0.12-mm thick. The full plant was 29 cm tall (the height above the post, see Fig. 2c). The materials used in the model plant were chosen to mimic the dynamic behavior of live *Spartina alterniflora* leaves and stem (Table 1). The plant material rigidity, *EI*, was tested on an Instron 5965 unit from INSTRON (Norwood, MA) applying the three-point bending test.

All experiments were conducted in a 24-m-long by 38-cm-wide wave flume (Fig. 3). Monochromatic waves with 2-s period were generated with a piston-type wave maker. A beach with a 1:5 slope was placed at the downstream end of the flume. The beach was covered with a 10-cm thick layer of coconut fiber which limited the wave reflection to $7\% \pm 3\%$ for the tested wave conditions. Four types of experiments were conducted to explore the dynamic reconfiguration of and drag on an individual leaf and stem, and on full model and live plants in waves (Fig. 2). In each experiment, a single live or model plant was attached to a short stainless steel post with 2 mm diameter, which was attached to a submersible force sensor (Futek LSB210 100g) (see Fig. 3). The force sensor was calibrated by National Instrument (NI-USB 9237) and the force measurements were logged to a computer through Labview. Based on calibration, the force measurements had an accuracy of 10% and a resolution of 0.0001 N. The force sensor was mounted beneath an acrylic ramp (1-m top length, 2-m bottom length, 13-cm height, and spanning the flume width) to avoid interaction between wave fluid motion and the sensor.

In experiment 1, the drag and motion of a single plastic leaf were measured under a range of waves (Table 2). The leaf was tested with different angles to the vertical, α , and rotated around the vertical to verify assumption 6, i.e. the force contribution from N_l leaves distributed both along and around the stem with angle α with respect to the vertical direction can be represented by the drag on a representative vertical leaf ($\alpha=0^{\circ}$). The base of each test leaf was attached to a small iron plate, which was fixed at $\alpha=0^{\circ}$ or 15° to vertical. This maintained a fixed angle at the base of the leaf, even as the upper part of the leaf reconfigured under wave motion. For $\alpha=0^{\circ}$, three initial postures were considered, with the leaf width oriented perpendicular, parallel, and at 45° to the wave propagation direction. Fig. 2a shows an example of an individual leaf with $\alpha=0^{\circ}$ and the leaf width parallel to wave propagation direction. In two additional postures, a leaf oriented with its width perpendicular to wave propagation direction was tilted 15° upstream and downstream. All five postures are included in Fig. 4 in the Results section.

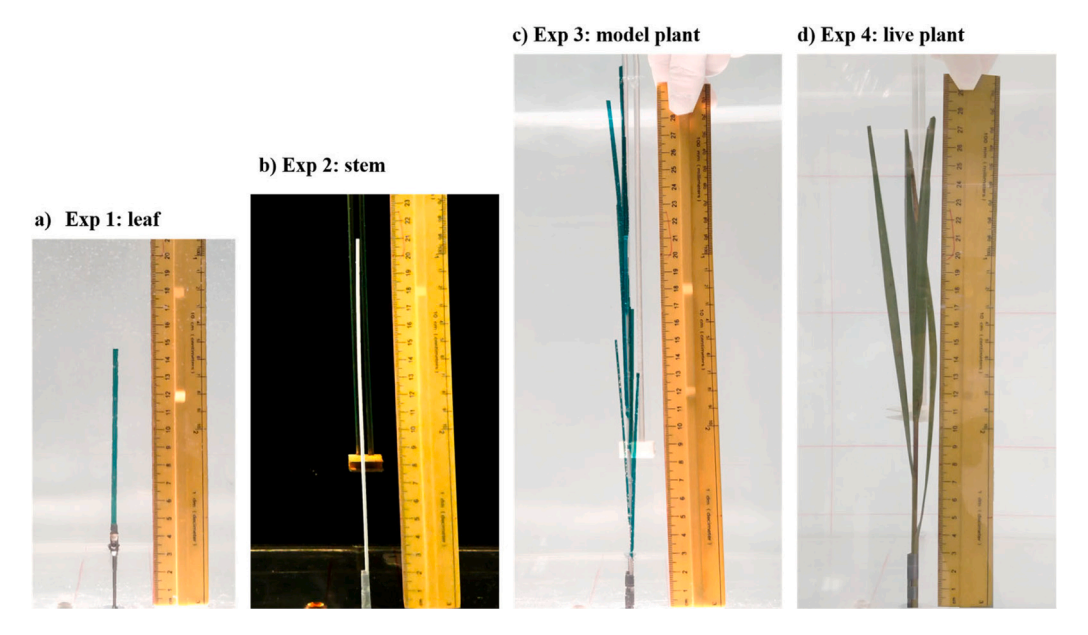


Fig. 2. (a) an individual vertical leaf with leaf width oriented parallel to incoming wave, (b) a plastic circular stem, (c) a model plant consisting of 10 leaves and a circular stem, and (d), a live Spartina alterniflora shoot.

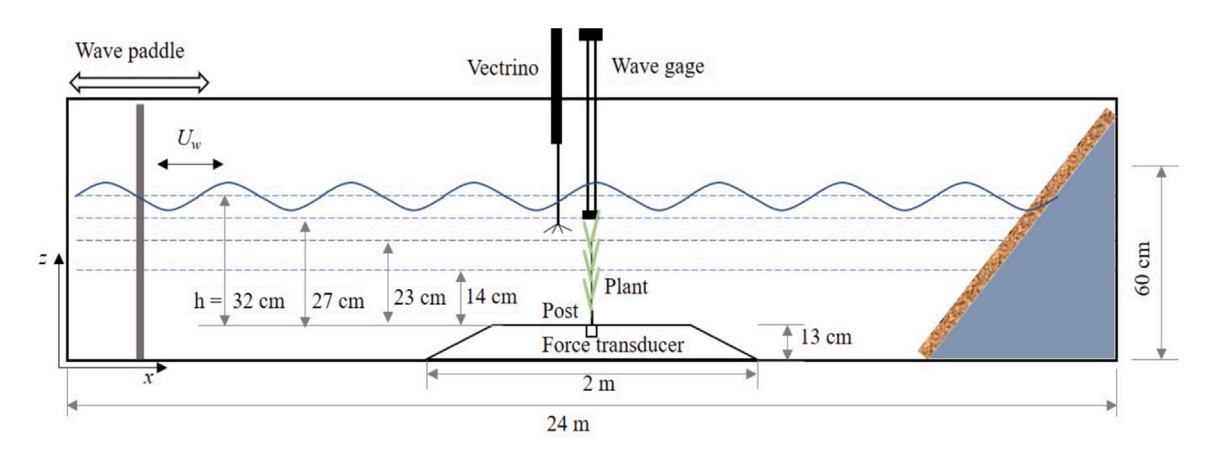


Fig. 3. Schematic of the experiment setup, not drawn to scale. The wave paddle is shown to the left and the beach to the right. The beach had a 1:5 slope and was covered with a layer of 10-cm thick coconut fiber. The model plant was attached to a submersible force sensor which was housed in an acrylic ramp. A wave gage recorded the free surface displacement at the same longitudinal position as the plant but with 9-cm lateral distance. A Nortek Vectrino+ was used to measure velocity profiles 10-cm upstream of the plant's position, but with the plant removed.

In experiment 2 (Fig. 2b), the motion of and the drag on the stem alone were measured under several wave conditions (Table 2). The material properties are listed in Table 1. Note that the stem length was the length of the stem above the post. Measurements from experiment 1 and experiment 2 were used to validate the dynamic model Eqs. (6) and (9) for an individual leaf and an individual stem ($N_I = 0$), respectively.

In experiment 3, the drag force on the full model plant was measured under several water depths, h = 14, 23, 27, and 32 cm above the ramp (see Fig. 3). Because the post lifted the model plant up by 2 cm, the corresponding submerged plant heights $h_{p,s}$ were 12, 21, 25, and 29 cm, respectively. For h = 32 cm, the plant was fully submerged. The contribution from the leaves and the stem to the plant scale drag was analyzed by comparing the drag measured on the leaf alone (experiment 1) and on the stem alone (experiment 2) to the full plant drag (experiment 3). These comparisons were also used to estimate the sheltering coefficient, C_s , in Eq. (9).

Finally, in experiment 4, measurements made on a live *Spartina alterniflora* plant (Fig. 2d) were used to validate the predictive model (Eqs. (6) and (9)). Individual plants were carefully dug out with roots and soil intact from Rumney Marsh Reservation in Massachusetts Bay, USA. Experiment 4 was conducted within 2 days after collection from the field. The roots were removed just before placement in the wave channel. After cutting, the plant was dry for only a few minutes

Table 1

Material properties of the live and model plants. The model plant used in experiment 3 was made of 10 leaves and one stem with the same properties as the individual leaf (experiment 1) and the individual stem (experiment 2), respectively. The live plant in experiment 4 has 5 leaves. l_l , b, d are the mean values with the standard deviations of leaf length, width, and thickness, respectively. The material rigidity, EI, was tested on an Instron 5965 using the three-point bending test. E was obtained by dividing EI by I.

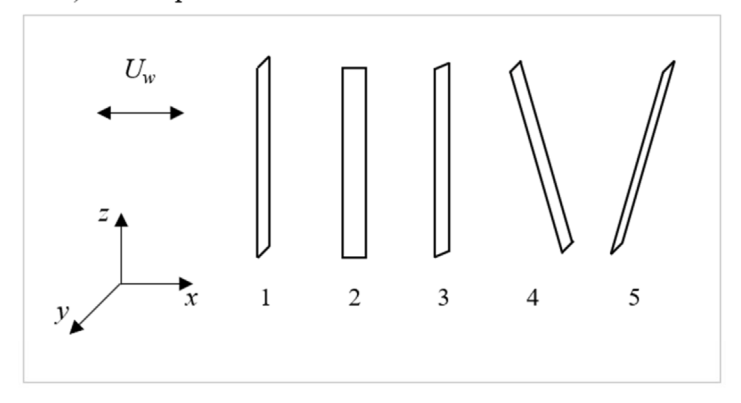
Model leaf	Model stem
$\rho_p = 1.35 \pm 0.06 \text{ g/cm}^3$	$\rho_p = 1.06 \pm 0.01 \text{ g/cm}^3$
$l_l = 10 \pm 0.2 \text{ cm}$	$l_{\rm s} = 19 \pm 0.2 {\rm cm}$
$b = 3 \pm 0.2 \text{ mm}$	$D = 2 \pm 0.01 \text{ mm}$
$d = 0.12 \pm 0.01 \text{ mm}$	
$I_l = 4.3 \times 10^{-16} \text{ m}^4$	$I_s = 7.9 \times 10^{-13} \text{ m}^4$
$E_l=4.8\pm0.4~\mathrm{GPa}$	$E_{\rm s} = 1.72 \pm 0.03 \; {\rm GPa}$
$E_l I_l = 2.07 \times 10^{-6} \text{ N m}^2$	$E_s I_s = 1.35 \times 10^{-3} \text{ N m}^2$
Live plant leaf	Live plant stem
Live plant leaf $\frac{\rho_p = 0.84 \text{ g/cm}^3}{l_l = 17 \pm 6 \text{ cm}}$	Live plant stem $\rho_p = 0.9 \text{ g/cm}^3$ $l_s = 16 \pm 0.2 \text{ cm}$
$\rho_p = 0.84 \text{ g/cm}^3$	$\rho_p = 0.9 \text{ g/cm}^3$
$ \rho_p = 0.84 \text{ g/cm}^3 $ $ l_l = 17 \pm 6 \text{ cm} $	$ \rho_p = 0.9 \text{ g/cm}^3 $ $ l_s = 16 \pm 0.2 \text{ cm} $
$ ho_p = 0.84 \text{ g/cm}^3$ $l_l = 17 \pm 6 \text{ cm}$ $b = 6.4 \pm 1 \text{ mm}$	$ \rho_p = 0.9 \text{ g/cm}^3 $ $ l_s = 16 \pm 0.2 \text{ cm} $
$ ho_p = 0.84 \text{ g/cm}^3$ $l_i = 17 \pm 6 \text{ cm}$ $b = 6.4 \pm 1 \text{ mm}$ $d = 0.48 \pm 0.08 \text{ mm}$	$ ho_p = 0.9 \text{ g/cm}^3$ $l_s = 16 \pm 0.2 \text{ cm}$ $D = 2.5 \pm 0.8 \text{ mm}$

Table 2

Wave conditions used in the experiments including water depth, h, wave amplitude, a_w , wave velocity, U_w , and wave excursion $A_w = U_w T_w/(2\pi)$, wave period was $T_w = 2.00 \pm 0.02$ s for all tests. The correspond nondimensional parameters B, Ca, and L are also summarized in the table. Experiments 1, 2, 3, and 4 correspond to experiments on an individual leaf, an individual stem, a full model plant, and a live plant, respectively.

cctively.						
·	$a_w \pm 0.1$ cm	1.1	1.7	2.4	3.3	4.2
h = 32 cm	$U_w \pm 1 \text{ cm/s}$	5	7	10	15	20
	$A_w \pm 0.1$ cm	1.6	2.2	3.2	4.8	6.4
R. — —0.6	Ca _l	3.0	7.7	17	33	57
$D_l = -0.0$	L_l	6.9	4.3	2.9	2.1	1.6
Exp1 to 3 $P = 0 \times 10^{-3}$	Ca_{s}	0.02	0.05	0.1	0.2	0.4
$D_{S} = -3 \times 10$	L_s	13	8.1	5.5	3.9	3
	$a_w \pm 0.1 \text{ cm}$	1.1	1.7	2.4	3.4	
h = 27 cm	$U_w \pm 1$ cm/s	6	8	14	19	
	$A_w \pm 0.1$ cm	1.9	2.6	4.5	6.1	
R. — —0.6	Ca_l	4.6	9.4	28	57	
$D_l = -0.0$	L_l	5.6	3.9	2.2	1.6	
$P = 0 \times 10^{-3}$	Ca_s	0.03	0.07	0.20	0.40	
$D_S = -9 \times 10^{-9}$	L_s	11	7.3	4.3	3.0	
	$a_w \pm 0.1~\mathrm{cm}$	1	1.6	2.5	3.1	
h = 23 cm	$U_w \pm 1$ cm/s	6	11	16	20	
	$A_w \pm 0.1$ cm	1.9	3.5	5.1	6.4	
$R_1 = -0.6$	Ca_l	4.5	16.3	39	58	
$D_l = 0.0$	L_l	5.6	2.9	1.9	1.6	
Exp3 $R = -9 \times 10^{-3}$	Ca_{s}	0.03	0.1	0.3	0.4	
$D_S = -3 \times 10$	$L_{\scriptscriptstyle S}$	11	5.6	3.6	3.0	
	$a_w \pm 0.1~\mathrm{cm}$	1.3	2	2.5		
h = 14 cm	$U_w \pm 1$ cm/s	8	14	19		
	$A_w \pm 0.1$ cm	2.6	4.5	6.1		
$R_1 = -0.6$	Ca_l	9.3	31	52		
$B_l = 0.0$	L_l	3.9	2.1	1.6		
$R = -2 \times 10^{-3}$	Ca_s	0.02	0.1	0.1		
$D_{\rm S} = -2 \times 10$	L_s	7.4	4.1	3.1		
	$a_w \pm 0.1~\mathrm{cm}$	1	1.6	2.1	2.9	3.9
h = 32 cm	$U_w \pm 1$ cm/s		7		14	18
	$A_w \pm 0.1$ cm	1.4	2.3	3.2	4.4	5.8
$B_{i} = -0.1$	Ca_l	0.36	0.95	2.1	4.1	7.1
$D_l = 0.1$	L_l	12	7.3		3.5	2.7
$R - 4 \times 10^{-7}$	Ca_{s}	0.02	0.04	0.09	0.2	0.3
D _S = 4 × 10	L_s	11	6.8	4.6	3.3	2.5
	$h = 32 \text{ cm}$ $B_{l} = -0.6$ $B_{s} = -9 \times 10^{-3}$ $h = 27 \text{ cm}$ $B_{l} = -0.6$ $B_{s} = -9 \times 10^{-3}$ $h = 23 \text{ cm}$ $B_{l} = -0.6$ $B_{s} = -9 \times 10^{-3}$ $h = 14 \text{ cm}$ $B_{l} = -0.6$ $B_{s} = -2 \times 10^{-3}$	$\begin{array}{llllllllllllllllllllllllllllllllllll$	$\begin{array}{c} a_w \pm 0.1 \ {\rm cm} \\ b = 32 \ {\rm cm} \\ & \begin{array}{c} a_w \pm 0.1 \ {\rm cm} \\ U_w \pm 1 \ {\rm cm/s} \\ A_w \pm 0.1 \ {\rm cm} \\ \end{array} \begin{array}{c} 5 \\ A_w \pm 0.1 \ {\rm cm} \\ \end{array} \begin{array}{c} 3.0 \\ L_l \\ 6.9 \\ 0.02 \\ L_s \\ \end{array} \begin{array}{c} 3.0 \\ 0.02 \\ L_s \\ \end{array} \begin{array}{c} Ca_s \\ 13 \\ \end{array} \\ \begin{array}{c} a_w \pm 0.1 \ {\rm cm} \\ \end{array} \begin{array}{c} 1.1 \\ W_w \pm 1 \ {\rm cm/s} \\ \end{array} \begin{array}{c} 6 \\ A_w \pm 0.1 \ {\rm cm} \\ \end{array} \begin{array}{c} 1.1 \\ W_w \pm 1 \ {\rm cm/s} \\ \end{array} \begin{array}{c} 6 \\ A_w \pm 0.1 \ {\rm cm} \\ \end{array} \begin{array}{c} 1.1 \\ W_w \pm 1 \ {\rm cm/s} \\ \end{array} \begin{array}{c} 6 \\ A_w \pm 0.1 \ {\rm cm} \\ \end{array} \begin{array}{c} 1.1 \\ W_w \pm 1 \ {\rm cm/s} \\ \end{array} \begin{array}{c} 6 \\ W_w \pm 0.1 \ {\rm cm} \\ \end{array} \begin{array}{c} 1.1 \\ W_w \pm 1 \ {\rm cm/s} \\ \end{array} \begin{array}{c} 6 \\ W_w \pm 0.1 \ {\rm cm} \\ \end{array} \begin{array}{c} 1.1 \\ W_w \pm 1 \ {\rm cm/s} \\ \end{array} \begin{array}{c} 6 \\ W_w \pm 0.1 \ {\rm cm} \\ \end{array} \begin{array}{c} 1.1 \\ W_w \pm 1 \ {\rm cm/s} \\ \end{array} \begin{array}{c} 6 \\ W_w \pm 0.1 \ {\rm cm} \\ \end{array} \begin{array}{c} 1.1 \\ W_w \pm 1 \ {\rm cm/s} \\ \end{array} \begin{array}{c} 6 \\ W_w \pm 0.1 \ {\rm cm} \\ \end{array} \begin{array}{c} 1.1 \\ W_w \pm 1 \ {\rm cm/s} \\ \end{array} \begin{array}{c} 8 \\ W_w \pm 0.1 \ {\rm cm} \\ \end{array} \begin{array}{c} 1.1 \\ W_w \pm 1 \ {\rm cm/s} \\ \end{array} \begin{array}{c} 8 \\ W_w \pm 0.1 \ {\rm cm} \\ \end{array} \begin{array}{c} 1.1 \\ W_w \pm 1 \ {\rm cm/s} \\ \end{array} \begin{array}{c} 8 \\ W_w \pm 0.1 \ {\rm cm} \\ \end{array} \begin{array}{c} 1.1 \\ W_w \pm 1 \ {\rm cm/s} \\ \end{array} \begin{array}{c} 3.9 \\ W_w \pm 0.1 \ {\rm cm} \\ \end{array} \begin{array}{c} 1.1 \\ W_w \pm 1 \ {\rm cm/s} \\ \end{array} \begin{array}{c} 3.9 \\ W_w \pm 0.1 \ {\rm cm} \\ \end{array} \begin{array}{c} 1.1 \\ W_w \pm 1 \ {\rm cm/s} \\ \end{array} \begin{array}{c} 3.9 \\ W_w \pm 0.1 \ {\rm cm} \\ \end{array} \begin{array}{c} 1.1 \\ W_w \pm 1 \ {\rm cm/s} \\ \end{array} \begin{array}{c} 4.1 \\ W_w \pm 1 \ {\rm cm/s} \\ \end{array} \begin{array}{c$	$\begin{array}{c} h = 32 \text{ cm} & \begin{array}{c} a_w \pm 0.1 \text{ cm} \\ U_w \pm 1 \text{ cm/s} \\ A_w \pm 0.1 \text{ cm} \\ \end{array} \begin{array}{c} 5 \\ 7 \\ A_w \pm 0.1 \text{ cm} \\ \end{array} \begin{array}{c} 1.6 \\ 2.2 \\ \end{array} \\ B_l = -0.6 & \begin{array}{c} Ca_l \\ L_l \\ Ca_s \\ Ca_s \\ Ca_s \\ \end{array} \begin{array}{c} 0.02 \\ 0.05 \\ Ca_s \\ A_w \pm 0.1 \text{ cm} \\ \end{array} \begin{array}{c} 1.1 \\ 1.7 \\ Ca_s \\ C$	$\begin{array}{c} h = 32 \text{ cm} & \begin{array}{c} a_w \pm 0.1 \text{ cm} \\ U_w \pm 1 \text{ cm/s} \\ A_w \pm 0.1 \text{ cm} \\ \end{array} & \begin{array}{c} 1.1 \\ U_w \pm 1 \text{ cm/s} \\ A_w \pm 0.1 \text{ cm} \\ \end{array} & \begin{array}{c} 1.6 \\ 1.6 \\ \end{array} & \begin{array}{c} 2.2 \\ 3.2 \\ \end{array} & \begin{array}{c} 3.2 \\ \end{array} \\ B_l = -0.6 \\ B_s = -9 \times 10^{-3} \\ Ca_s \\ L_s \\ \end{array} & \begin{array}{c} Ca_s \\ 0.002 \\ 0.05 \\ 0.1 \\ L_s \\ \end{array} & \begin{array}{c} 13 \\ 8.1 \\ 5.5 \\ \end{array} & \begin{array}{c} 8.1 \\ 5.5 \\ \end{array} \\ h = 27 \text{ cm} \\ \end{array} & \begin{array}{c} a_w \pm 0.1 \text{ cm} \\ U_w \pm 1 \text{ cm/s} \\ A_w \pm 0.1 \text{ cm} \\ \end{array} & \begin{array}{c} 1.1 \\ 1.7 \\ 1.7 \\ \end{array} & \begin{array}{c} 2.4 \\ 4.5 \\ 4.5 \\ \end{array} \\ B_l = -0.6 \\ B_s = -9 \times 10^{-3} \\ Ca_s \\ L_s \\ \end{array} & \begin{array}{c} Ca_s \\ 0.03 \\ 0.07 \\ 0.20 \\ Ca_s \\ 0.03 \\ 0.07 \\ 0.20 \\ \end{array} & \begin{array}{c} 0.20 \\ 0.20 \\ 0.20 \\ \end{array} \\ h = 23 \text{ cm} \\ \end{array} & \begin{array}{c} Ca_s \\ U_w \pm 1 \text{ cm/s} \\ A_w \pm 0.1 \text{ cm} \\ 0.1 \\ \end{array} & \begin{array}{c} 1 \\ 1.6 \\ 0.2.5 \\ \end{array} & \begin{array}{c} 0.03 \\ 0.07 \\ 0.20 \\ 0.20 \\ \end{array} \\ B_l = -0.6 \\ Ca_l \\ L_l \\ 0.56 \\ 0.03 \\ 0.1 \\ 0.3 \\ 0.1 \\ 0.3 \\ 0.1 \\ 0.3 \\ 0.01 \\ 0.3 \\ 0.01 \\ 0.3 \\ 0.01 \\ 0.3 \\ 0.01 \\ 0.3 \\ 0.01 \\ 0.3 \\ 0.01 \\ 0.3 \\ 0.01 \\ 0.3 \\ 0.02 \\ 0.01 \\ 0.01 \\ 0.02 \\ \end{array} \\ h = 14 \text{ cm} \\ \begin{array}{c} a_w \pm 0.1 \text{ cm} \\ U_w \pm 1 \text{ cm/s} \\ A_w \pm 0.1 \text{ cm} \\ 0.02 \\ 0.02 \\ 0.01 \\ 0.01 \\ 0.01 \\ 0.01 \\ 0.01 \\ 0.02 \\ 0.02 \\ 0.04 \\ 0.09 \\ \end{array} \\ \begin{array}{c} 0.02 \\ 0.02 \\ 0.04 \\ 0.09 \\ 0.00 \\ 0.0$	$\begin{array}{c} h = 32 \text{ cm} & \begin{array}{c} a_w \pm 0.1 \text{ cm} \\ U_w \pm 1 \text{ cm/s} \\ A_w \pm 0.1 \text{ cm} \\ \end{array} & \begin{array}{c} 1.1 \\ U_w \pm 1 \text{ cm/s} \\ A_w \pm 0.1 \text{ cm} \\ \end{array} & \begin{array}{c} 1.6 \\ 0.22 \\ 0.32 \\ \end{array} & \begin{array}{c} 3.2 \\ 3.2 \\ \end{array} & \begin{array}{c} 4.8 \\ \end{array} \\ B_l = -0.6 \\ B_s = -9 \times 10^{-3} \\ Ca_s \\ L_s \\ \end{array} & \begin{array}{c} Ca_s \\ 0.02 \\ 0.05 \\ 0.1 \\ 0.2 \\ 0.05 \\ \end{array} & \begin{array}{c} 0.1 \\ 0.1 \\ 0.2 \\ 0.05 \\ 0.1 \\ 0.2 \\ 0.05 \\ 0.1 \\ 0.2 \\ 0.05 \\ 0.1 \\ 0.2 \\ 0.05 \\ 0.1 \\ 0.2 \\ 0.1 \\ 0.2 \\ 0.05 \\ 0.1 \\ 0.2 \\ 0.02 \\ 0.05 \\ 0.1 \\ 0.2 \\ 0.1 \\ 0.2 \\ 0.05 \\ 0.1 \\ 0.2 \\ 0.2 \\ 0.1 \\ 0.2 \\ 0.2 \\ 0.1 \\ 0.2 $

a). Tested postures of leaf



b). Maximum drag force on varies postures of leaf

Fig. 4. Drag force measured on a single leaf. (a) The tested postures of the leaf and (b) the maximum drag force plotted against the wave velocity squared. For postures 1, 2, and 3, $\alpha = 0^{\circ}$ and the leaf width is aligned perpendicular, parallel, and at 45° to the wave direction, respectively. Posture 1 tilted 15° to upstream (or downstream) produced posture 4 (or posture 5). Note that the force measurements for postures 4 (squares) and 5 (diamonds) overlap.

0.02

 U_w^2 (m²s⁻²)

0.03

0.04

-0.001

0

0.01

before being submerged in the flume. The tests were finished within 8 h after the plant was cut. The live plant parameters and the tested wave conditions are listed in Tables 1 and 2, respectively.

For each experiment under each flow condition, drag force and wave height were measured simultaneously with a sampling rate of 2000 Hz and for a duration of 3 min. For each wave condition, a separate force measurement was made on the post alone (without plant), and the force on the post was subtracted from the force measured with the plant and post together. During each force measurement, a smart cellphone (MIX 2S) camera was used to record a 10-s UHD 4k video at 30 fps which covered 5 wave periods. The camera was fixed to a tripod through a self-stick holder. 100 photos with 0.1 s intervals were extracted from the videos to obtain plant dynamic posture. For each plant, a photo with a ruler beside the plant (Fig. 2) was taken and used to calculate the scale (pixels/cm) of the photo using MATLAB.

For the force measurements, the FFT (fast Fourier transform) method in MATLAB was used to filter out high-frequency noise. The angular frequency $\omega = 2\pi/T_w$ was determined using the 4th-order Fourier fitting in MATLAB. For sampling frequency f_{samp} , there were $\gamma = 2\pi/\omega f_{samp}$ samples and thus γ phase bins in each wave period (Lei and Nepf, 2019). Each 3-min record contained $M = 180/T_w$ wave periods. The phase averaged force in the nth phase bin (n = 1 to γ), which

corresponded to phase $\phi = 2\pi n/\gamma$, was defined as,

$$\check{F}\left(\phi\left(n\right)\right) = \frac{1}{M} \sum_{m=0}^{M-1} F(n + \gamma m) \tag{10}$$

The same phase average method was applied to the wave gage records to obtain the phase averaged water surface displacement, $\check{\eta}$ (ϕ (n)). The wave amplitude a_w was calculated from the root-mean-square surface displacement, $a_w = \sqrt{\frac{2}{\gamma} \sum_{n=1}^{\gamma} \check{\eta}} (\phi(n))^2$.

After the force measurements were completed, the plant and force sensor were removed, and an acoustic Doppler velocimeter (Nortek Vectrino+) was used to measure velocity profiles at 10 cm upstream of the position where the plant had been to avoid the influence of the hole through which the plant attached to the force sensor. The vertical resolution of the velocity profiles was 1 cm. At each measurement point, the Vectrino recorded a 2-min record at 200 Hz sampling frequency. The velocity measurement was quality checked and despiked within each phase bin with the methods described in Nikora and Goring (2000) and Goring and Nikora (2002). The phase averaged velocity $\check{u}(\phi(n))$ was calculated by similar method as Eq. (10). The wave velocity U_w was represented by the root-mean-square velocity, i.e. $U_w = \sqrt{\frac{2}{\gamma}} \sum_{n=1}^{\gamma} \check{u}^2$.

The decrease in drag force associated with plant reconfiguration was characterized by an effective length. The effective length of each element (leaf or stem) normalized by its full length, l_e/l , was calculated from the measured drag force and the drag force estimated for the rigid element (Lei and Nepf, 2019), i.e.,

$$\frac{l_e}{l} = \frac{F_{d,max}}{F_{r,max}} = \frac{\text{the measured maximum force}}{\text{the expected maximum force on a rigid counter part}}$$
 (11)

in which $F_{d,max}$ and $F_{r,max}$ were defined as,

$$F_{d,max} = \frac{\left| \max(\check{F}(\phi)) \right| + \left| \min(\check{F}(\phi)) \right|}{2} \tag{12}$$

$$F_{r,max} = \frac{1}{2} \rho C_D A(U_w)^2 \tag{13}$$

in which C_D for the stem and leaf were estimated from previous experiments on cylinders and plates, respectively, in waves. The drag coefficient depends on KC ($KC_S = U_w T_w/D$ for the stem and $KC_l = U_w T_w/b$ for the leaf) (Keulegan and Carpenter, 1958; Luhar and Nepf, 2016; Sarpkaya and O'Keefe, 1996). Specifically, $C_D = \max(1, 2.9KC_S^{-0.2})$ for the stem, and $C_D = \max(1.95, 10KC_l^{-1/3})$ for the leaves. Note that the same C_D values were used in the predictive model. $A = Dl_S$ and $A = bl_l$ are the frontal area for the stem and the leaf, respectively. The absolute value in Eq. (12) is needed because the force changes sign over the wave period. $F_{r,max}$ had an estimated uncertainty of 15% based on a 10% estimated uncertainty of C_D and a 8% variation in C_D over the water depth.

The drag predicted by the marsh plant dynamic model (Eqs. (6) and (9)) was validated using the experimental measurements. For the model prediction of the full plant, Eq. (6) was applied first to calculate the force on a single vertical leaf. The leaf force was then put into Eq. (9) to calculate the drag on the full plant. The sheltering coefficient C_s in Eq. (9) was determined based on drag force measured on an individual leaf, an individual stem, and on the full plant. A constant skin friction $C_f = 0.1$ was used in all model predictions following Luhar and Nepf (2016). Similar to C_D , the inertial coefficient C_M for the stem and the leaves were also estimated from experimental measurements for a cylinder and a plate based on the KC number (Keulegan and Carpenter, 1958; Sarpkaya and O'Keefe, 1996). Specifically, $C_M = 0.2KC_s^{0.55}$ for the stem and $C_M = 0.48KC_l^{0.47}$ for the leaf were inferred from the literature specifically for KC > 25, consistent with the conditions in the current study. When the plant was emergent, i.e. water depth less than the full plant height (Experiment 3), the submerged plant length $h_{p,s}$ varied with the wave surface displacement through the wave cycle. To account for this in modeling, the submerged height of the plant and the number of leaves contributing to the plant drag was estimated at each step according to wave phase. After validation, the predictive model (Eqs. (6) and (9)) was first used to explore a range of conditions that align with field conditions, and then applied to explore the drag on different marsh species and their wave damping potential.

4. Results

4.1. Influence of leaf posture on leaf drag

The drag force measured on individual leaves was influenced by the posture of the leaf (Fig. 4, posture 1 to 5). The leaf drag was maximum when the leaf was tilted toward the upstream (posture 4) or downstream (posture 5) relative to the incoming wave (Fig. 4b). As expected, due to the symmetry in the wave velocity, postures 4 and 5 produced the same maximum drag. The higher drag on tilted blades was associated with a reduced range of motion. For example, Fig. 5 shows the range of postures over one wave cycle for a leaf with posture 1 (vertical) and posture 5 (tilted 15° downstream at the

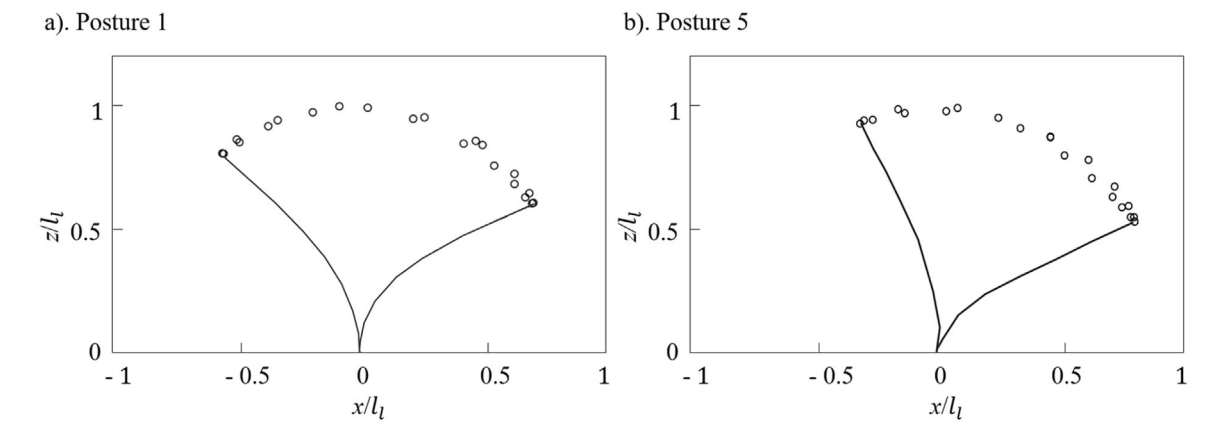


Fig. 5. Comparison of leaf motion over one wave cycle with (a) leaf posture 1 and (b) leaf posture 5 under 32-cm water depth, 2-s wave period, and 4.2-cm wave amplitude. In each subfigure, curves show the limit of the leaf motion and the circles show the tips of the leaf over one wave cycle with 0.1-s time interval.

leaf base). The average height over one wave cycle was about the same for a leaf with posture 1 and posture 5. However, the tip excursion of posture 5 was 14% smaller than that of posture 1. The smaller leaf motion was associated with a higher relative motion between the fluid and the leaf, and thus higher drag (Fig. 4b). The minimum drag was measured for posture 2, a vertical leaf with the leaf width oriented parallel to the wave direction. In the wave conditions tested here, this leaf remained parallel to the wave direction, but this would be less likely for more flexible or longer leaves or when the hydraulic force is more intense such that the leaf would be twisted over (Gosselin, 2019; Vogel, 2007). For these reasons, posture 2 was less representative of real leaves. Considering the other postures, the drag measured on the vertical blade orientated perpendicular to the wave (posture 1) was a representative average amongst the other postures (Fig. 4). Given this, we proposed that it would be reasonable to represent the average force of multiple leaves distributed along a stem with different juncture angles by the force predicted for a leaf oriented in posture 1, i.e. vertical at the base and width perpendicular to the wave. Hereafter, the leaf alone experiment (exp 1) will refer to a leaf with posture 1.

4.2. Reconfiguration of and drag on individual plant elements

The wave-induced drag on an individual leaf (experiment 1) and on the stem alone (experiment 2) both followed the scaling law developed in previous studies (Lei and Nepf, 2019; Luhar and Nepf, 2016), specifically, $l_e/l = (CaL)^{-1/4}$ (Fig. 6a). The motion of a stem and a leaf over one wave period and for increasing wave amplitude (1.1 to 4.2 cm) is shown in Fig. 6b and c, respectively. The circles in Fig. 6b and c indicate the tips of the stem and leaf extracted from the videos. The gray curves show the stem (Fig. 6b) and leaf (Fig. 6c) postures predicted by the model Eqs. (6) and (9), respectively, with $N_l = 0$ in Eq. (9), that is no leaves. For the tested wave conditions, the individual stem exhibited limited motion which was far less than the wave orbital diameter (shown with horizontal lines in Fig. 6b). In particular, for $a_w = 4.2$ cm, the wave orbital diameter was 12.8 cm (67% stem length), the corresponding stem tip excursion diameter was 5% the stem length. In contrast, the tip of the leaf moved over a distance comparable to the wave orbital diameter, indicating nearly passive motion, which reduced the drag, relative to a rigid leaf (Fig. 6c). The excursion of the leaf tip became greater when the wave amplitude increased. In fact, the horizontal excursion of the leaf tip was greater than the horizontal wave orbital diameter (Fig. 6c). This can be explained by the contribution of the vertical wave velocity. The horizontal orbital diameter defines translation associated only with the horizontal wave velocity. However, the vertical component of wave velocity can also impact the translation of the leaf tip. Specifically, after the passage of a wave crest, as the horizontal wave velocity approaches zero, the vertical wave velocity is downward, which depresses the leaf downward, a movement that is associated with some additional forward motion of the leaf tip (see Figure 52 in Mancheño, 2016).

An interesting observation is that the stem experienced elevated drag relative to a stationary cylinder for CaL < 1 (Fig. 6a). Specifically, the drag on the flexible stem was 68% higher than a rigid stem for CaL = 0.3 ($a_w = 1.1$ cm). For this case, the stem force spectrum exhibited a peak at the wave frequency (0.5 Hz), as expected, but also at 2 Hz, which was close to the stem's first-mode natural frequency (1.8 Hz, based on Table 8.1 in Blevins, 1979). A vibration higher than the wave frequency, but of smaller amplitude than that of direct wave induced motion, was also observed in the stem. These observations were consistent with vortex-induced vibration, which has been previously documented to enhance drag on cylindrical structures (e.g., Gabbai and Benaroya, 2005; Gopalkrishnan, 1993; So et al., 2000) and on plants (e.g., de Langre, 2006; Païdoussis et al., 2010; Py et al., 2006)

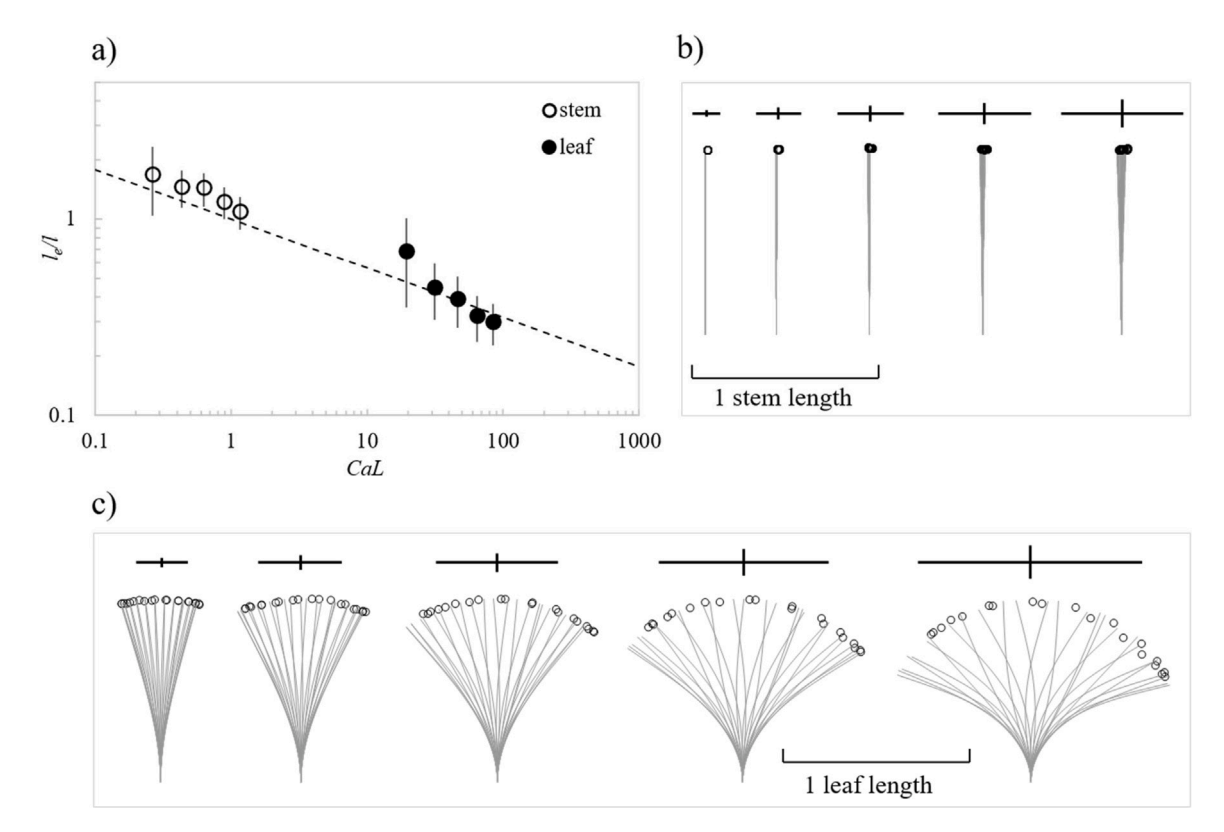


Fig. 6. (a) Ratio of effective length (l_e) to full length, which is equivalent to the ratio of drag force on a flexible element to that on a rigid element of length l, plotted against CaL for the stem alone (open circles, experiment 2) and the individual leaf (closed circles, experiment 1 posture 1). The error bars represent the standard deviation of measured drag over 90 wave periods and a 15% estimated uncertainty for the rigid drag force, $F_{r,max}$. The dash line indicates the scaling law $l_e/l = (CaL)^{-1/4}$ (Lei and Nepf, 2019; Luhar and Nepf, 2016). (b) Motion of the stem and (c) motion of the leaf, both for increasing wave amplitude: left to right $a_w = 1.1$, 1.7, 2.4, 3.3, and 4.2 cm. The circles in (b) and (c) indicate the observed positions of the stem and leaf tip, and the gray curves are the model predicted stem postures and leaf postures over one wave cycle. The solid black lines are wave orbital diameter in horizontal (–) and vertical (1) direction.

4.3. Motion of and drag on flexible model plant with leaves

Experiment 3 examined the motion of and drag on the full model plant. The plant motion through one wave period is shown in Fig. 7. First, because the drag on the leaves was transmitted to the stem, the drag on and motion of the stem increased, relative to the stem alone (Fig. 6b). Specifically, for the same wave (4.2-cm amplitude), the tip excursion diameter increased from 5% of the stem length without leaves (Fig. 6b) to 20% with leaves (Fig. 7). Second, interaction between individual leaves and between leaves and stem diminished the motion of the leaves. Specifically, compared to the excursion of a single leaf (Fig. 6c), the excursion of leaves attached to the stem was much smaller, and, the motion of each leaf was limited to the side of its attachment point. For example, the leaves attached to the upstream side of the stem easily deflected toward the upstream under the wave trough, but exhibited limited or no deflection toward the downstream under the crest. In contrast, the stem deflected similarly in the upstream (trough) and downstream (crest) directions.

The maximum drag on the model plant, individual stem, and individual leaf are shown in Fig. 8a. The model predictions of the force on the leaf (dashed line, Eq. (6)) and stem (dotted line, Eq. (9)) are also included and show good agreement with the measured drag with no calibration. The leaf component of plant-scale drag was estimated as the difference between the drag on the full plant and the drag on the stem. The leaves contributed $72\% \pm 1\%$ of the plant-scale drag across all wave amplitudes considered, $a_w = 1.1$ to 4.2 cm. However, since the leaves reconfigure more significantly than the stem, the leaf contribution may decrease at higher wave velocity. For example, this has been observed for trees exposed to uni-directional current. Specifically, because the leaves reconfigure to a greater degree than the stems and branches, the fractional contribution of leaf drag decreases with increasing current speed (e.g. Jalonen and Järvelä, 2013; Västilä and Järvelä, 2014; Whittaker et al., 2013; Wilson et al., 2008, 2010; Xavier et al., 2010). In this study, leaves contributed the majority of the drag which highlighted the importance of correctly capturing the leaf reconfiguration and its impact on plant scale drag. The full plant had ten leaves. However, the drag force on the plant, $F_{d,plant}$, was smaller than the sum of stem drag, $F_{d,stem}$, and 10 times the drag on an individual leaf, $F_{d,leaf}$. This was likely due to sheltering and interaction

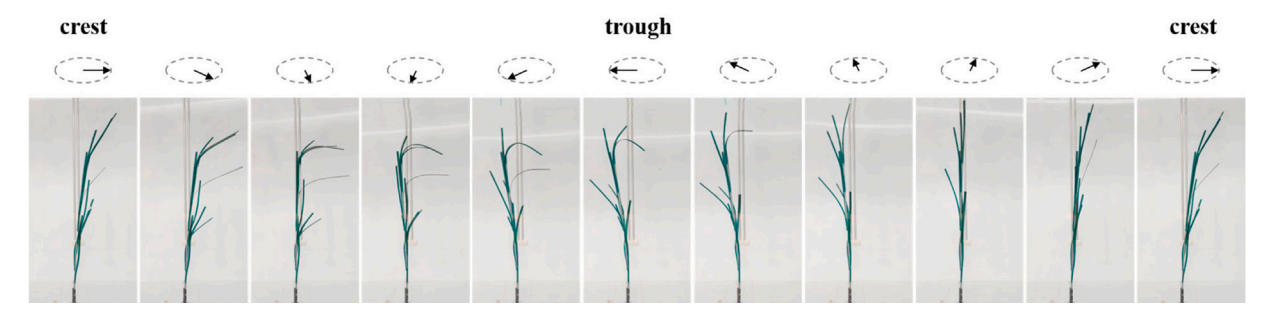


Fig. 7. The motion of a model plant over one wave cycle. The water depth was 32 cm, wave period was 2 s and the wave amplitude was 4.2 cm. From left to right, the wave went from crest to trough and to crest with 0.2-sec time interval. The dashed oval illustrates the full wave orbital, with individual arrows showing the wave velocity vector for each image.

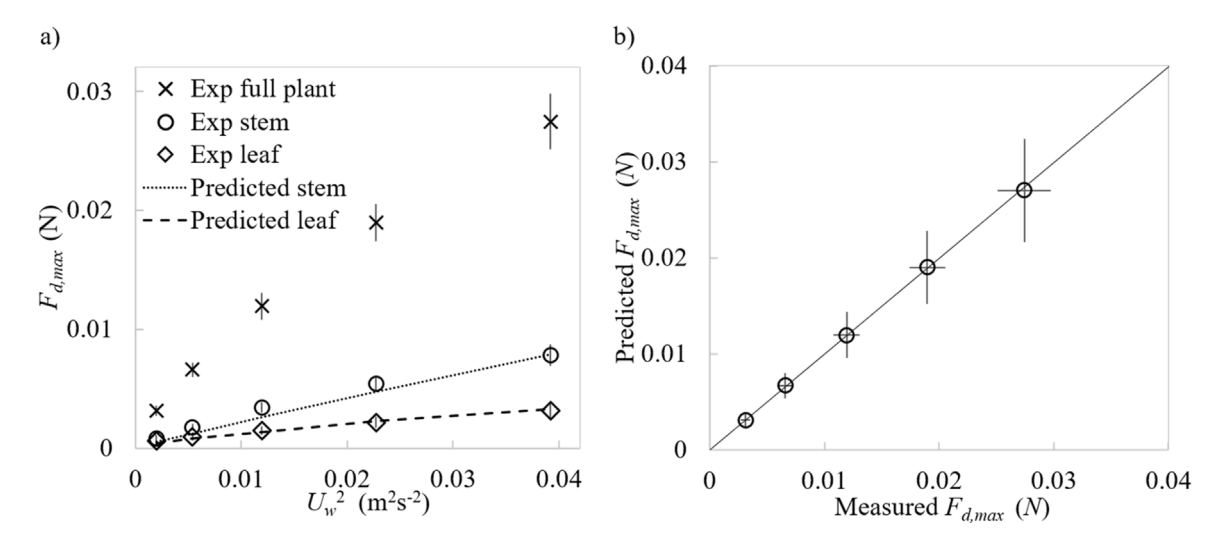


Fig. 8. (a) The drag force measured on the full plant (crosses), the stem (circles), and an individual leaf (diamonds). Curves show the predicted drag for an individual leaf (dashed curve, Eq. (6)) and the stem alone (dotted curve, Eq. (9) with $N_l = 0$). (b) Drag predicted by Eqs. (6) and (9) with $C_s = 0.6$ plotted against measured plant drag. The measured drag uncertainty is represented by the standard deviation of $F_{d,max}$ among the measured wave periods. The prediction of the full plant drag had an estimated uncertainty of 20% based on 10% estimated uncertainty in C_D , 8% in wave orbital velocity, 20% in C_s , and the standard deviations of the model plant geometrical and mechanic properties (see Table 1).

among the stem and leaves. The degree of leaf sheltering, i.e. the value of C_s , was estimated by fitting the measured drag: $F_{d,plant} = F_{d,stem} + (0.6 \pm 0.1)N_lF_{d,leaf}$. Consistent with this, choosing the sheltering coefficient $C_s = 0.6$ in Eq. (9) produced a prediction of the full plant drag force that agreed with the measured value within uncertainty (Fig. 8b).

4.4. Motion of and drag on live salt marsh plant

The live *Spartina alterniflora* exhibited similar wave-induced motion as the model plant (Fig. 9). Specifically, with the leaves attached, the stem moved with the waves, but the stem had negligible wave-induced motion when the leaves were cut. However, the live plant leaves stayed closer together than the model plant leaves (Fig. 7) suggesting that the sheltering might be greater (smaller C_s). Consistent with this, the drag on the live plant was over-predicted by the model using $C_s = 0.6$ (Fig. 10a). The prediction was improved by using $C_s = 0.4$ (Fig. 10b). This is a bit counter-intuitive, as one might expect that the live plant with fewer leaves (5) would experience less sheltering (larger C_s) than the model plant with more leaves (10). However, the leaves of the live plant were more rigid (Table 1), which kept them more closely aligned to the vertical, enhancing the leaf-to-leaf sheltering.

4.5. Simplified prediction for the drag force on a marsh plant

The good agreement shown in Sections 4.3 and 4.4 supported the model assumptions made in Section 2, specifically, the leaves wrap and distribute around the stem can be represented by a vertical flat leaf and C_s adequately quantified the drag reduction due to the sheltering and interaction among the leaves and the stem. The model Eqs. (6) and (9) provide an

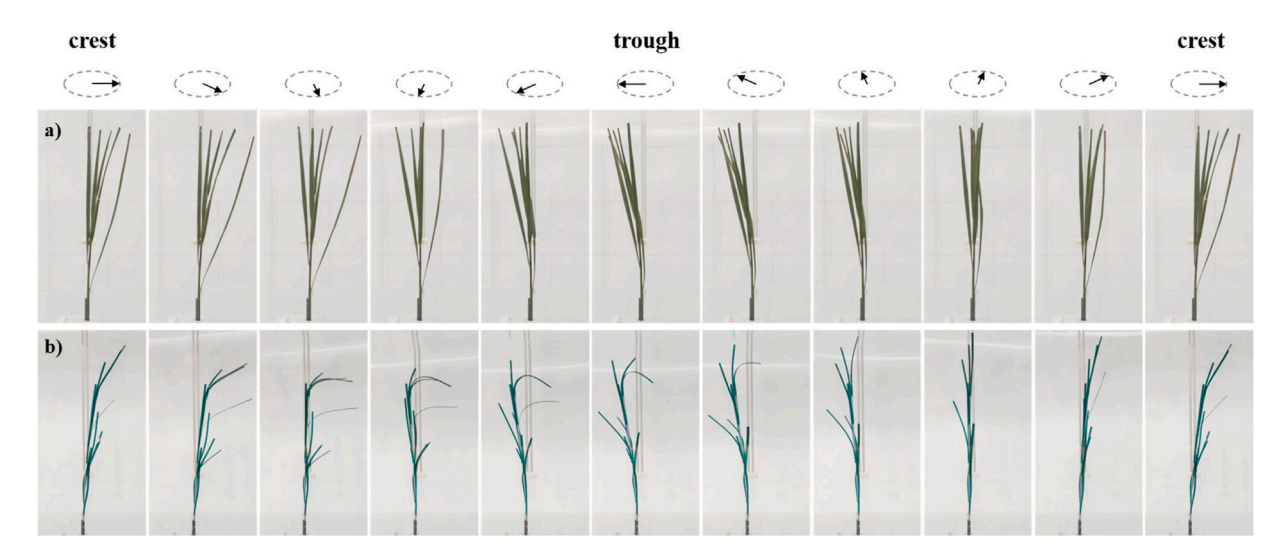


Fig. 9. (a) The motion of a live *Spartina alterniflora* shoot over one wave cycle for h = 32 cm, $T_w = 2$ s, and $a_w = 3.9$ cm. From left to right, the wave went from crest to trough and to crest with 0.2-sec time interval. The dashed oval illustrates the full wave orbital, with individual arrows showing the wave velocity vector for each image. (b) The motion of the model plant over the wave cycle which is the same as Fig. 7.

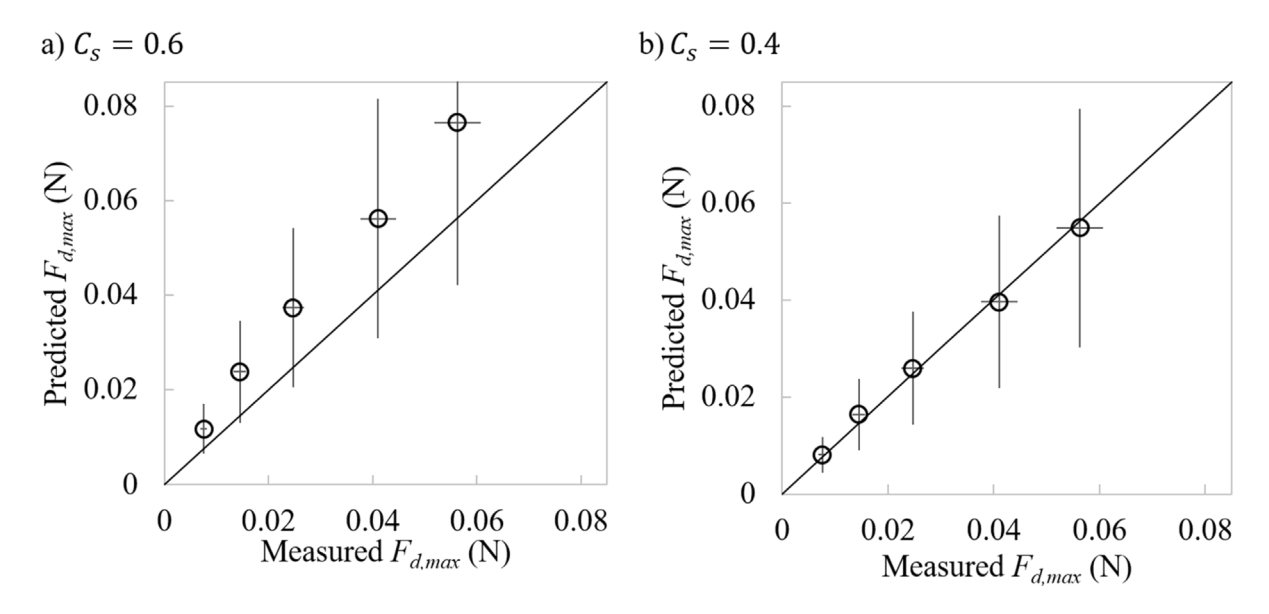


Fig. 10. The maximum drag predicted by Eqs. (6) and (9) versus the maximum measured drag force $F_{d,max}$ for the live *Spartina alterniflora* with (a) $C_s = 0.6$ and (b) $C_s = 0.4$. The solid lines indicate 1:1 ratio. The error in measured drag was estimated from the standard deviations of $F_{d,max}$ among 90 measured wave periods. The predictions had an estimated uncertainty of 45% based on a 20% uncertainty in C_s , 10% estimated uncertainty in the drag coefficient C_D , 8% in wave velocity, and the standard deviations of the model plant geometrical and mechanic properties (see Table 1).

accurate, but cumbersome, prediction of the drag on a marsh plant. In this section, a simplified prediction, more useful for application in the field, is developed and validated. Recall that the drag on an individual leaf and individual stem followed the previously derived scaling law, $F_e/F_r = (CaL)^{-1/4}$ (Lei and Nepf, 2019; Luhar and Nepf, 2016). For marsh plants with a central stem and multiple leaves, such as *Spartina alterniflora*, we propose that the maximum, wave-induced plant-scale drag can be estimated from a sum of the leaf and stem drag, accounting for the leaf sheltering. Specifically,

$$F_{d,plant} = C_s N_l F_{d,leaf} + F_{d,stem} = \underbrace{C_s N_l F_{r,max,l} (Ca_l L_l)^{-1/4}}_{leaf\ drag} + \underbrace{F_{r,max,s} (Ca_s L_s)^{-1/4}}_{stem\ drag}$$
(14)

in which $F_{r,max,l}$ and $F_{r,max,s}$ are the maximum wave-induced drag force for a rigid leaf and stem, respectively, which can be estimated by Eq. (13). Based on the original scaling (Luhar and Nepf, 2016), Eq. (14) represents conditions with CaL > 1. Specifically, Ca > 1 (the element bends) and L > 1 (the wave excursion is less than the element length).

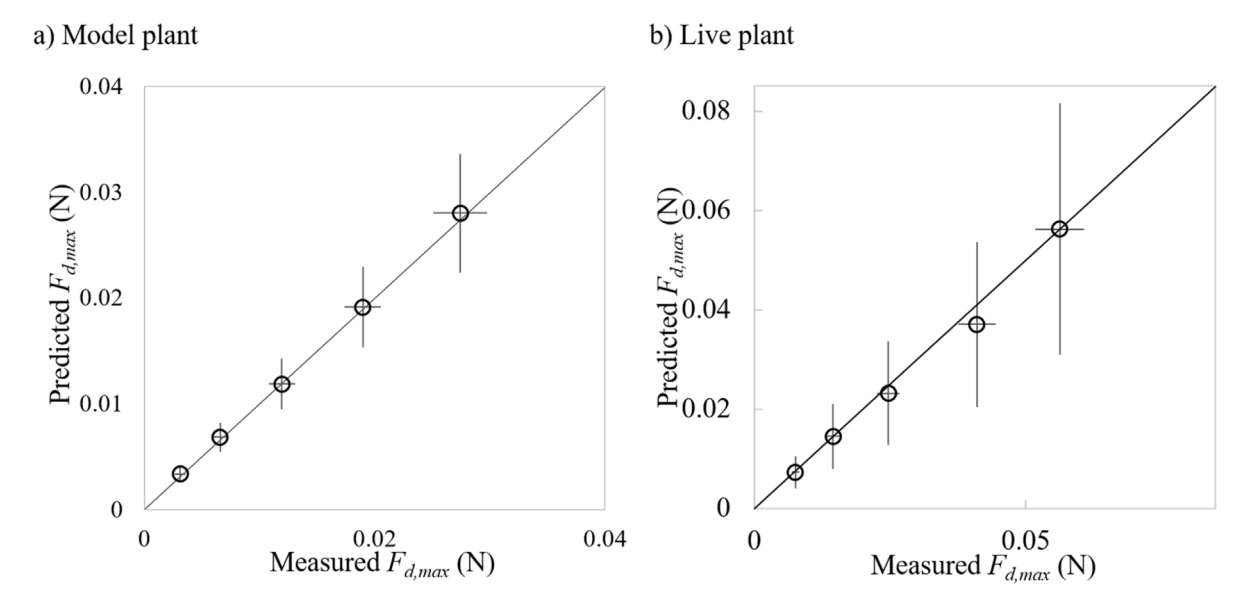


Fig. 11. The maximum drag predicted by the simplified drag law described in Eq. (14) versus the measured drag force for (a) the model plant using $C_s = 0.6$ and (b) the live *Spartina alterniflora* using $C_s = 0.4$. The error bars in measured force reflects the standard deviations over 90 wave periods and the error bars in the predicted force reflects uncertainty in C_s , C_D , U_w , and the plant parameters.

However, experiments conducted here suggested it can also represent conditions with Ca_sL_s as small as 0.3 (Fig. 6). Note that the plant buoyancy was neglected in Eq. (14). This is reasonable because the Buoyancy number was much smaller than 1 based on Eq. (1) and a typical range of marsh plant morphology ($l_l = 10$ to 50 cm, $l_s = 30$ to 200 cm, d = 0.1 to 0.7 mm, and D = 2 to 10 mm), material density ($|\Delta \rho| < 200 \text{ kg/m}^3$), and elastic modulus (0.1~10 GPa). For example, the Buoyancy number for the live plant specimen (experiment 4) was $B_l = 0.1$ and $B_s = 4 \times 10^{-7}$ (Table 1). Eq. (14) was validated by comparing the predicted drag to the measured drag on the model plant (Fig. 11a) and also on the live plant (Fig. 11b). In both cases, the prediction agreed with the measurement within uncertainty. Over the range of wave conditions considered, the simplified prediction (Eq. (14)) was comparable to the full prediction by Eqs. (6) and (9), which is shown by comparing Figs. 8b and 10b to 11a and b, respectively.

4.6. Drag force variation with the plant submergence

In experiment 3, the drag force per submerged plant length was examined for plants submerged 41%, 72%, 86%, and 100% of the total plant height. The measured drag per submerged plant length was not a function of submerged water depth as long as the wave orbital velocity was the same. Specifically, the drag per submerged length measured for four different depths was the same within uncertainty at each wave condition (diamonds in Fig. 12a). The predicted drag (Eqs. (6) and (9)) captured this feature (circles in Fig. 12a), because it assumed a uniformly distributed leaf drag acting on the stem. The lack of depth dependence in the drag per plant length was consistent with the uniform distribution of plant leaves along the stem (Figs. 1 and 7).

The plant drag increased with velocity more slowly than quadratic (Fig. 12a). Specifically, for $U_w < 0.2$ m/s (Fig. 12a), the measurements suggested $F_{d,max}/h_{p,s} \sim U_w^{1.2\pm0.3}$. Further, over this range of wave orbital velocity, the simplified model and the full model predictions (solid line and cross symbol, respectively, in Fig. 12a) has the same trend.

Recall that the single leaf and stem followed the dependence $F_{d,max}/F_{r,max} \sim (CaL)^{1/4}$ (see Fig. 6a), which is equivalent to $F_{d,max} \sim C_D U_w^{1.75}$. The weaker dependence on U_w of the measured and predicted drag on the full plant was due to the fact that the drag coefficient C_D for the leaves and the stem decreased with increasing U_w , and this dependence was excluded from Ca, because C_D does not appear in Ca. Recall that, $C_D = \max(1, 2.9KC_s^{-0.2})$ for the stem, and $C_D = \max(1.95, 10KC_l^{-1/3})$ for the leaves (based on Keulegan and Carpenter, 1958), which has the embedded velocity dependence of $C_D \sim U_w^{-0.2}$ and $C_D \sim U_w^{-1/3}$, respectively. However, C_D reached its minimum value (1 or 1.95 for the stem and leaf, respectively) at $U_w > 0.2$ m/s and for this range of velocity the simplified model (Eq. (14)) predicted $F_{d,max} \sim U_w^{1.75}$, as expected based on the scaling $F_{d,max}/F_{r,max} \sim (CaL)^{-1/4}$ (see solid line for $U_w > 0.2$ m/s in Fig. 12b). The full model (Eqs. (6) and (9)) also predicted $F_{d,max} \sim U_w^{1.75}$ over the range $U_w = 0.2$ m/s to 0.3 (cross symbol in Fig. 12), however at higher wave velocity ($U_w > 0.3$ m/s), the full model predicted $F_{d,max}/h_{p,s} \sim U_w^{1.0\pm0.2}$, deviating from the simplified model. The deviation of the simplified model (Eq. (14)) from the full model (Eqs. (6) and (9)) was attributed to the feedback from leaf drag to stem motion, which was not reflected in the simplified model.

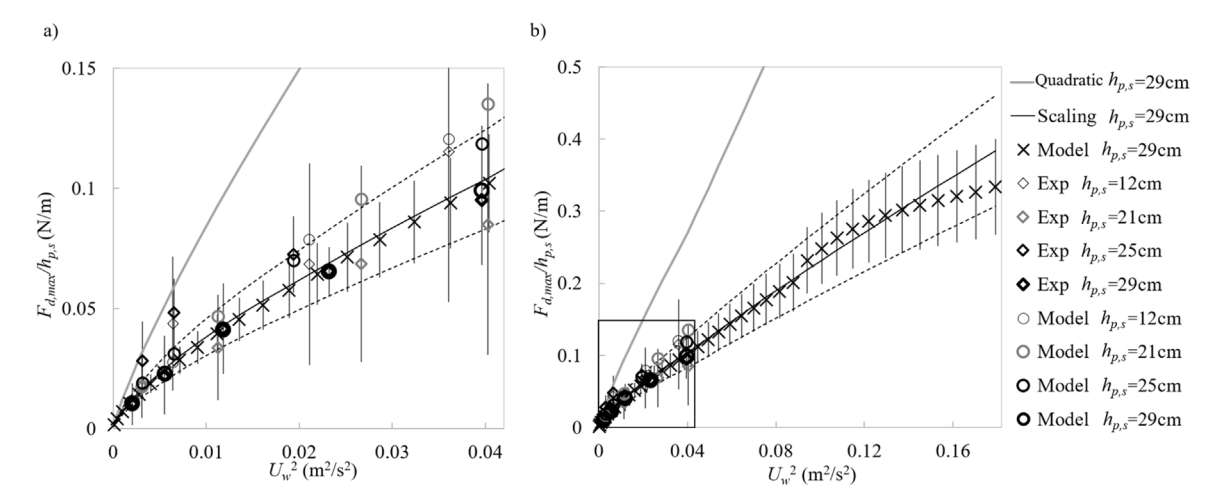


Fig. 12. Measured and predicted drag force per submerged plant length versus wave velocity squared. (a) is a close up of the boxed area in (b). Drag was measured for the full plant for $h_{p,s} = 12$, 21, 25, and 29 cm (diamonds). The full plant height was 29 cm. Model (Eqs. (6) and (9)) predictions (circles) were made for the same plant submergence and wave velocities. In addition, predictions were made for h = 100 cm with $a_w = 0.5$ to 20 cm, using the full model (Eqs. (6) and (9)) and the simplified model (Eq. (14)), shown by the crosses and solid curve, respectively. $C_s = 0.6$ was applied for all predictions. The error in the measured data represent the standard deviations of $F_{d,max}$ over 90 wave periods, and 20% uncertainty in the prediction reflects uncertainty in C_s , C_D , U_w , and plant parameters. The dash curves are 20% uncertainty in the scaling law (Eq. (14)) prediction. For comparison, a quadratic drag relation is shown with thin gray curve.

Finally, while the full model captures the impact of leaf drag on stem reconfiguration, it did not explicitly model the impact of stem reconfiguration on leaf drag. The possible decrease in leaf drag associated with the pronation of the stem is represented within the sheltering coefficient, C_s . For this reason, the sheltering coefficient determined for the conditions in this study, with a small degree of stem reconfiguration (stem tip excursion diameter of 20% stem length), may lead to over-prediction in drag for conditions with larger stem reconfiguration. Up to wave velocity $U_w = 0.4$ m/s, the deviation between the simplified model and the full model was less than 15%. Given that both models had 20% uncertainty, the simplified model is considered to be accurate enough to explore variation in wave forces amongst different morphology, as we do in the discussion section.

5. Discussion

5.1. Wave induced drag force on different marsh plant species

Plant morphology and mechanical properties vary greatly among marsh plant species (Table 3). For example, *Scirpus maritimus* (also called *Bolboschoenus maritimus*) and *Scirpus tabernaemontani* (also called *Schoenoplectus tabernaemontani* as reported in Smith and Yatskievych, 1996) are two pioneer species that have very different morphology. The first one has a triangular stem cross-section and multiple leaves, while the later has an elliptical stem cross-section with no leaves (Heuner et al., 2015). In marsh plants with leaves, the leaf thickness spans from 0.1 mm to 0.7 mm (Maricle et al., 2009). The stem diameter of marsh plants varies from 2 mm (e.g. *Scirpus mariqueter* reported by Wang et al., 2016) to 15 mm (e.g. *Phragmites australis* reported by Nada et al., 2015), and the corresponding second moment of area ranges from 8 × 10⁻¹³ to 1 × 10⁻⁹ m⁴. The plant leaf and stem dimensions also vary within a species at different sites and during different seasons (Ritterbusch, 2007). The elastic modulus of most marsh grass stems span 0.1 to 32 GPa (Evans et al., 2007) (see Table 3). To explore the role of plant morphology on wave drag, typical plant parameters of five common marsh species (Table 3) were chosen to compare their wave damping potential. Due to a lack of reports on the stiffness of salt marsh leaves, the measured elastic modulus for *Spartina alterniflora* (Table 1), $E_I = 3$ GPa, was used for leaves of all species. In addition, a leaf thickness of d = 0.3 mm, which is the mean of the leaf thickness of 7 marsh species (Maricle et al., 2009), was used for all species.

The simplified model (Eq. (14)) was used to compare the plant scale drag on the species listed in Table 3 for a range of water depth (0.2 to 3 m). $C_s = 0.6$ was used because the mature marsh plants have similar morphology as the geometrically- and dynamically-scaled model plant (see photos of plants in Lövstedt and Larson (2010), Rupprecht (2015), Schoutens et al. (2020) and Fig. 2c), so that it is reasonable to assume the same sheltering. The wave amplitude varied with water depth. Specifically, based on many field conditions, the wave amplitude was set to be 0.2 times the water depth (Vuik et al., 2016). Wave period was set to be 4 s, within the range of wave period often reported for coastal regions, i.e. 2–5 s (Chen et al., 2005; Jadhav and Chen, 2013; Moeller et al., 1996; Paquier et al., 2019). The wave velocity U_w was calculated by the linear wave theory.

Table 3Plant parameters for five marsh species at mature growth. The full names are *Phragmites australis*, *Scirpus maritimus*, *Scirpus tabernaemontani*, *Spartina alterniflora*, and *Spartina anglica*, respectively.

Species	l_s	D	N _s	l_l	b	d	N _l	Es	E_sI_s	E_lI_l
	cm	mm	m^{-2}	cm	mm	mm	leaves	GPa	N m ²	N m ²
P. australis ^{1–6}	150	8	200	30	20	0.3	15	5	1	1.4×10^{-4}
S. maritimus ^{7–11}	120	8	400	40	8	0.3	8	0.97	0.072	5.4×10^{-5}
S. tabernaemontani ^{7,11}	120	9	700	-	_	-	0	0.13	0.042	-
S. alterniflora ^{12–19}	100	8	200	40	14	0.3	10	1.4	0.28	4.4×10^{-4}
S. anglica ^{9-10,13,19-20}	70	5	300	30	8	0.3	8	0.5	0.015	5.4×10^{-5}

Parameters were chosen based on data sources marked upright to the species name, where the corresponding references are Ostendorp and Möller (1991)¹, Boar et al. (1999)², Nada et al. (2015)³, Cho et al. (2017)⁴, Xi et al. (2017)⁵, Schaefer (2019)⁶, Heuner et al. (2015)⁷, Silinski et al. (2015)⁸, Vuik et al. (2016)⁹, Vuik et al. (2018)¹⁰, Schoutens et al. (2020)¹¹, Knutson et al. (1982)¹², Zhi et al. (2007)¹³, Feagin et al. (2011)¹⁴, Ysebaert et al. (2011)¹⁵, Yang et al. (2012)¹⁶, Jadhav and Chen (2013)¹⁷, Wu et al. (2016)¹⁸, Rupprecht (2015)¹⁹, Maricle et al. (2009)²⁰. Note that the leaf width was the width at leaf base. S. maritimus has a triangular cross section shape and the diameter listed in the table is the length of each side.

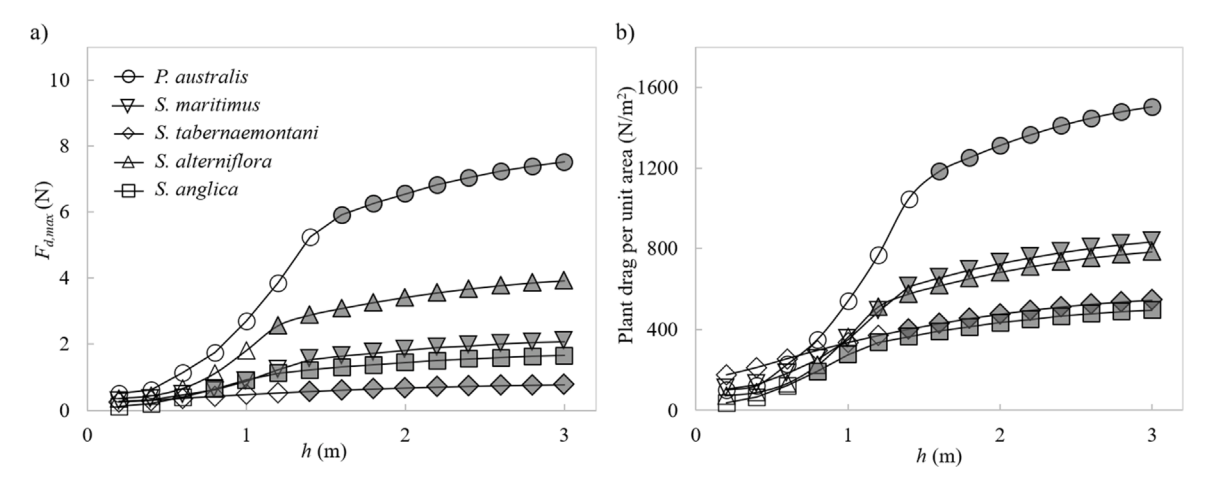


Fig. 13. (a) The simplified model (Eq. (14)) predicted drag force on a single plant for five marsh species for h = 0.2 to 3 m, wave period of 4 s, and wave amplitude $a_w = 0.2$ h. (b) Drag force generated by unit area marsh meadow with the density of plants N_s listed in Table 3. Open symbols correspond to emergent plant conditions, and filled symbols correspond to submerged plant conditions.

As expected, the drag on an individual plant (Fig. 13a) depends on the plant morphology. *Phragmites australis* (circles), with many big leaves, greatest rigidity, and greatest plant height, experienced the highest drag force. In contrast, the short, flexible *Scirpus tabernaemontani* (diamonds) with no leaves, experienced much smaller drag, just 10% to 50% the drag on *Phragmites australis*. The *Spartina alterniflora* (upward-pointing triangles) fell in between these two extremes.

Water depth had a significant influence on the plant drag (Fig. 13a). Drag increased rapidly with depth when the plant was emergent (open symbols) and increased more slowly once the plant was submerged (filled symbols). The continued increase in drag once the plant was submerged was due to the assumption that wave amplitude was linked to water depth, which is consistent with field observations. Under small water depths ($h \le 0.4$ m), only a few leaves on the leaved species contributed to the plant drag, such that $F_{d,max}$ differed by only 5% between the leaved *Scirpus maritimus* (downward-pointing triangles) and the *Scirpus tabernaemontani* (diamonds) with no leaves. However, for $h \ge 1.4$ m both species were submerged and the contribution of leaves significantly increased the drag on *Scirpus maritimus*, relative to the *Scirpus tabernaemontani* without leaves. Specifically, drag on *Scirpus maritimus* was 167% greater than that of *Scirpus tabernaemontani* for h > 1.4 m.

Plant shoot density is also important when calculating the total force generated per bed area within a marsh and hence the wave damping potential (Fig. 13b). When the shoot density was considered, the order of species in terms of plant drag per bed area (Fig. 13b) was shifted relative to the ordering of species in terms of drag on an individual plant (Fig. 13a). For example, $F_{d,max}$ for an individual *Scirpus maritimus* (downward triangle) was 1/2 of that for an individual *Spartina alterniflora* (upward triangle), but the drag per unit bed area in *Scirpus* marsh was 6% greater than that of *Spartina alterniflora* marsh. This highlights the importance of marsh plant density, in addition to plant morphology.

The model can also be used to explore the previous suggestion that biomass and plant surface area can provide a prediction of wave damping (Friedland and Denny, 1995; Paul et al., 2012, 2016; Rupprecht, 2015). To explore this point, the biomass and the total surface area of each species were estimated for h = 2 m with a constant plant material density $\rho_p = 1000 \text{ kg/m}^3$ for all species. The biomass was calculated as plant volume times material density. The surface area was calculated as the sum of stem frontal area and one-sided leaf area. The plant surface area had a strong positive correlation to the predicted plant drag per unit bed area (Fig. 14), $R^2 = 0.95$, but the biomass did not have a significant correlation

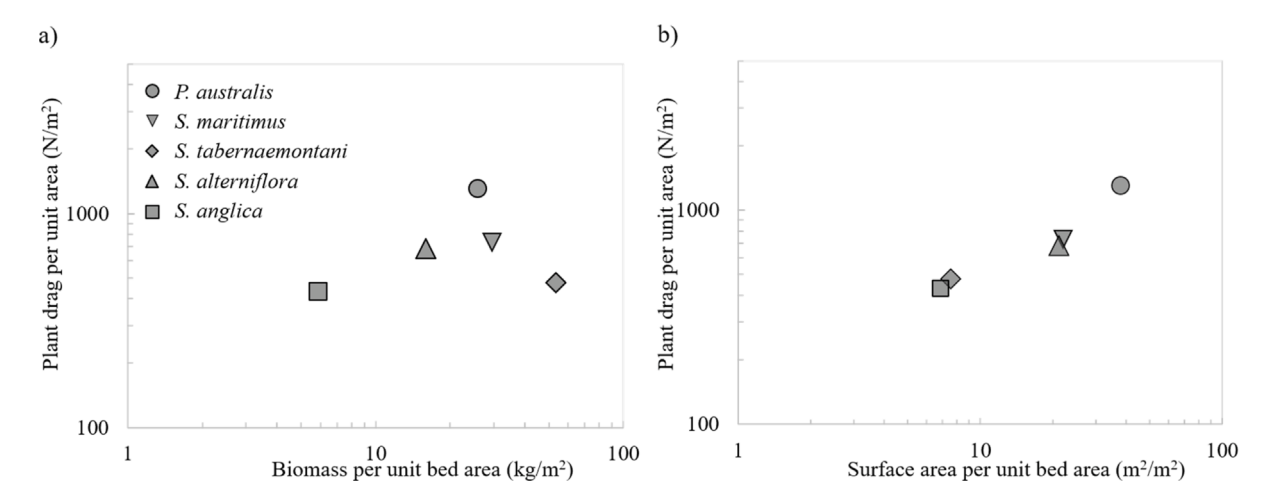


Fig. 14. Plant drag per unit area versus (a) plant biomass and (b) plant surface area per unit bed area for h = 2 m and all species were submerged. The correlation between the drag per unit area to biomass and to surface area per unit area are 0.001 and 0.95, respectively.

to the drag per unit bed. For example, at h=2 m, *Scirpus tabernaemontani* (diamond) had 8 times the biomass of *Spartina anglica* (square) but only a 10% difference in drag per unit bed. However, if one only makes comparison among plants with the same morphology, biomass understandably showed a significant correlation with drag per unit area. Specifically, $R^2=0.94$ between biomass and drag per unit bed area if only *Phragmites australis* (circle), *Spartina alterniflora* (upward-pointing triangle), and *Spartina anglica* (square) are considered, because these species have similar morphology (multiple leaves and one circular stem).

Recent studies have suggested that plants with different morphology grow within different ecological niches within a marsh because of the difference in their exposure to wave drag. For example, *Scirpus tabernaemontani* grows directly adjacent to the shore-ward edge of the marsh, while *Scirpus maritimus* grows more land-ward (Heuner et al., 2015; Schoutens et al., 2020). Schoutens et al. (2020) revealed that the greater flexibility and absence of leaves in *Scirpus tabernaemontani* gives it an advantage in the region of stronger waves at the edge of the marsh, because its morphological traits result in less drag on individual plants. This was confirmed by our model predictions, which showed that for the same wave conditions, the drag on an individual *Scirpus tabernaemontani* was less than *Scirpus maritimus* (Fig. 14a). Schoutens et al. (2020) suggested that following cooperative feedback between plants. The band of *Scirpus tabernaemontani* at the marsh edge reduces the wave condition inland, creating conditions where a plant with greater frontal area, such as *Scirpus maritimus*, can survive.

6. Conclusion

Nature-based solutions for coastal resilience involve the engineering and management of coastal marshes as a first line of defense against coastal flooding. A key component of this defense is the attenuation of waves. This study developed a theoretic model to describe the motion of and drag on marsh plants with leaves distributed along a central stem. Experiments with live and plastic mimics supported the leaf and stem components of the model, as well as the full plant model. For the tested conditions, the leaves contribute more than 70% of the plant drag. Because the leaves are distributed uniformly along the stem, the drag force per plant length was not a function of submergence depth. The model and experiments together confirmed that the plant geometric and mechanical properties, including the number of leaves, leaf length, width, and thickness, stem length and diameter, and the elastic modulus of the leaf and stem, are all factors that affect the wave induced motion of and drag on a marsh plant. To make precise prediction on wave attenuation, these plant properties have to be considered. Finally, a simplified prediction of marsh plant drag based on previous scaling laws for individual element reconfiguration was developed and validated. The simplified model provides a useful tool for assessing wave dissipation in the field, but which also reflects the reconfiguration and morphology of the plant.

CRediT authorship contribution statement

Xiaoxia Zhang: Conceptualization, Methodology, Software, Validation, Formal analysis, Investigation, Data curation, Writing - original draft, Visualization, Project administration, Funding acquisition. **Heidi Nepf:** Conceptualization, Resources, Writing - review & editing, Supervision, Project administration, Funding acquisition.

Declaration of competing interest

The authors declare that they have no known competing financial interests or personal relationships that could have appeared to influence the work reported in this paper.

Acknowledgments

We thank Dr. Juliet Simpson for assistance collecting live plants. We thank Dr. Jiarui Lei for his assistance with the wave channel. Funding was provided by US National Science Foundation EAR 1659923. Xiaoxia Zhang received support from the China Scholarship Council. Any opinions and conclusions are those of author(s) and do not necessarily reflect the views of the CSC or the US National Science Foundation.

Appendix. The symbols used in this paper

Α	Frontal area
A_w	Wave excursion (wave orbital radius)
a_w	Wave amplitude
В	Buoyancy number
b	Width of the blade or leaf
Ca	Wave Cauchy number
C_D	Drag coefficient
$C_{\rm f}$	Skin friction coefficient
C_M	Inertial coefficient
k'	Added mass coefficient
Cs	Sheltering coefficient
d d	Thickness of the blade or leaf
D D	Stem diameter
e	Natural logarithm constant
E	Young's modulus
_ F	Force on plant
f_{AM}	The added mass force per unit length
f_B	The buoyancy force per unit length
F_d	Drag force on plant
F_D	The drag force per unit length
$f_f^{\mathcal{L}}$	The skin friction per unit length
f_l	Force per stem length due to leaf
F_{samp}	Sampling frequency
f_{VB}	The virtual buoyancy per unit length
g	Gravitational acceleration
ĥ	Water depth
$h_{p,s}$	Submerged plant height
I	Second moment of area
KC	Keulegan–Carpenter number
1	Blade length
L	Ratio of blade length to wave excursion
l_e	Effective plant length
N_l	Number of leaves per stem
N_s	Number of stems per unit bed area
S	Curved coordinate along plant
t	Time
T	Tension
T_{l0}	Leaf exerted force on the stem-parallel direction
T_w	Wave period
и	Fluid velocity
U_w	Orbital wave velocity

V	The restoring force due to plant stiffness
V_{l0}	Leaf exerted force on the stem-normal direction
X	Coordinates in Cartesian coordinate system
α	Angle between leaf and stem
heta	Angle between plant and vertical
η	Water free surface displacement
ώ	Wave angular frequency
π	Constant 3.1415926
ho	Density of water
$ ho_{ m p}$	Density of the plant
Δho	The difference in density between water and plant
γ	Number of phase bins in one wave period
ϕ	Phase
Subscript	
1	Parameter associated with leaf
S	Parameter associated with stem
R	Relative parameter between flow and the plant
r	Parameter associated with rigid plant
max	Maximum value of the parameter
Other	
Õ Ô Ŏ	Tilde denotes complex variable in x and z direction
Ô	Hat denotes dimensionless parameter
Č)	Check denotes phase averaged variable
$\mathfrak{R}()$	Denotes the real component
$\mathfrak{I}()$	Denotes the imaginary component
l()	Absolute value

References

Anderson, M.E., Smith, J.M., 2014. Wave attenuation by flexible, idealized salt marsh vegetation. Coast. Eng. 83, 82–92. http://dx.doi.org/10.1016/j.coastaleng.2013.10.004.

Blevins, R.D.B., 1979. Formulas for Natural Frequency and Mode Shape. Van Nostrand Reinhold Company.

Boar, R.R., Kirby, J.J.H., Leeming, D.J., 1999. Variations in the quality of the thatching reed *Phragmites australis* from wetlands in East Anglia, England. Geol. Soc. Lond. Spec. Publ. 163, 145–151. http://dx.doi.org/10.1144/GSL.SP.1999.163.01.12.

Boesch, D.F., Turner, R.E., 1984. Dependence of fishery species on salt marshes: The role of food and refuge. Estuaries 7, 460–468. http://dx.doi.org/10.2307/1351627.

Bradley, K., Houser, C., 2009. Relative velocity of seagrass blades: Implications for wave attenuation in low-energy environments. J. Geophys. Res. 114, F01004. http://dx.doi.org/10.1029/2007|F000951.

Chen, Q., Zhao, H., Hu, K., Douglass, S.L., 2005. Prediction of wind waves in a shallow estuary. J. Waterw. Port Coast. Ocean Eng. 131, 137–148. http://dx.doi.org/10.1061/(ASCE)0733-950X(2005)131:4(137).

Cho, J.-S., Lee, J.-S., Kim, J.-W., 2017. Distribution of *Phragmites australis* communities with different habitat salinity. J. Coast. Res. 335, 1210–1216. http://dx.doi.org/10.2112/JCOASTRES-D-16-00065.1.

Cooper, N.J., 2005. Wave dissipation across intertidal surfaces in the wash tidal inlet, Eastern England. J. Coast. Res. 21, 28-40.

Dalrymple, R.A., Kirby, J.T., Hwang, P.A., 1984. Wave diffraction due to areas of energy dissipation. J. Waterw. Port Coast. Ocean Eng. 110, 67–79. http://dx.doi.org/10.1061/(ASCE)0733-950X(1984)110:1(67).

de Langre, E., 2006. Frequency lock-in is caused by coupled-mode flutter. J. Fluids Struct. 22, 783–791. http://dx.doi.org/10.1016/j.jfluidstructs.2006.

Evans, L.S., Kahn-Jetter, Z., Marks, C., Harmoney, K.R., 2007. Mechanical properties and anatomical components of stems of 42 grass species. J. Torrey Bot. Soc. 134, 458–467. http://dx.doi.org/10.3159/07-RA-009.1.

Feagin, R.A., Irish, J.L., Möller, I., Williams, A.M., Colón-Rivera, R.J., Mousavi, M.E., 2011. Short communication: Engineering properties of wetland plants with application to wave attenuation. Coast. Eng. 58, 251–255. http://dx.doi.org/10.1016/j.coastaleng.2010.10.003.

Friedland, M.T., Denny, M.W., 1995. Surviving hydrodynamic forces in a wave-swept environment: Consequences of morphology in the feather boa kelp, Egregia menziesii (Turner). J. Exp. Mar. Biol. Ecol. 190, 109–133. http://dx.doi.org/10.1016/0022-0981(95)00038-S.

Gabbai, R.D., Benaroya, H., 2005. An overview of modeling and experiments of vortex-induced vibration of circular cylinders. J. Sound Vib. 282, 575–616. http://dx.doi.org/10.1016/j.jsv.2004.04.017.

Gedan, K.B., Kirwan, M.L., Wolanski, E., Barbier, E.B., Silliman, B.R., 2011. The present and future role of coastal wetland vegetation in protecting shorelines: answering recent challenges to the paradigm. Clim. Change 106, 7–29. http://dx.doi.org/10.1007/s10584-010-0003-7.

Gopalkrishnan, R., 1993. Vortex-Induced Force on Oscillating Bluff Cylinders. Massachusetts Institute of Technology. Woods Hole Oceanographic Institution, USA.

Goring, D.G., Nikora, V.I., 2002. Despiking acoustic doppler velocimeter data. J. Hydraul. Eng. 128, 117–126. http://dx.doi.org/10.1061/(ASCE)0733-9429(2002)128:1(117).

Gosselin, F.P., 2019. Mechanics of a plant in fluid flow. J. Exp. Bot. 70, 3533-3548. http://dx.doi.org/10.1093/jxb/erz288.

Heuner, M., Silinski, A., Schoelynck, J., Bouma, T.J., Puijalon, S., Troch, P., Fuchs, E., Schröder, B., Schröder, U., Meire, P., Temmerman, S., 2015. Ecosystem engineering by plants on wave-exposed intertidal flats is governed by relationships between effect and response traits. PLoS ONE 10, e0138086. http://dx.doi.org/10.1371/journal.pone.0138086.

Jadhav, R.S., Chen, Q., 2013. Probability distribution of wave heights attenuated by salt marsh vegetation during tropical cyclone. Coast. Eng. 82, 47–55. http://dx.doi.org/10.1016/j.coastaleng.2013.08.006.

Jalonen, J., Järvelä, J., 2013. Impact of tree scale on drag: Experiments in a towing tank. In: Proceedings of 2013 IAHE World Congress.

Keulegan, G.H., Carpenter, L.H., 1958. Forces on cylinders and plates in an oscillating fluid. J. Res. Natl. Bur. Stand. 60, 423. http://dx.doi.org/10.6028/

Knutson, P.L., Brochu, R.A., Seeling, W.N., Margaret, I., 1982. Wave damping in spartina alterniflora marsh. Wetlands 2, 87-104.

Koftis, T., Prinos, P., Stratigaki, V., 2013. Wave damping over artificial *Posidonia oceanica* meadow: A large-scale experimental study. Coast. Eng. 73, 71–83. http://dx.doi.org/10.1016/j.coastaleng.2012.10.007.

Lei, J., Nepf, H., 2019. Wave damping by flexible vegetation: Connecting individual blade dynamics to the meadow scale. Coast. Eng. 147, 138–148. http://dx.doi.org/10.1016/j.coastaleng.2019.01.008.

Lövstedt, C.B., Larson, M., 2010. Wave damping in reed: Field measurements and mathematical modeling. J. Hydraul. Eng. 136, 222–233. http://dx.doi.org/10.1061/(ASCE)HY.1943-7900.0000167.

Luhar, M., Infantes, E., Nepf, H., 2017. Seagrass blade motion under waves and its impact on wave decay. J. Geophys. Res. Oceans 122, 3736–3752. http://dx.doi.org/10.1002/2017|C012731.

Luhar, M., Nepf, H.M., 2011. Flow-induced reconfiguration of buoyant and flexible aquatic vegetation. Limnol. Oceanogr. 56, 2003–2017. http://dx.doi.org/10.4319/lo.2011.56.6.2003.

Luhar, M., Nepf, H.M., 2016. Wave induced dynamics of flexible blades. J. Fluids Struct. 61, 20-41.

Mancheño, A.G., 2016. Interaction Between Wave Hydrodynamics and Flexible Vegetation. Delft University of Technology.

Maricle, B.R., Koteyeva, N.K., Voznesenskaya, E.V., Thomasson, J.R., Edwards, G.E., 2009. Diversity in leaf anatomy, and stomatal distribution and conductance, between salt marsh and freshwater species in the C4 genus *Spartina* (Poaceae). New Phytol. 184, 216–233. http://dx.doi.org/10. 1111/j.1469-8137.2009.02903.x.

Mcleod, E., Chmura, G.L., Bouillon, S., Salm, R., Björk, M., Duarte, C.M., Lovelock, C.E., Schlesinger, W.H., Silliman, B.R., 2011. A blueprint for blue carbon: toward an improved understanding of the role of vegetated coastal habitats in sequestering CO₂. Front. Ecol. Environ. 9, 552–560. http://dx.doi.org/10.1890/110004.

Méndez, F.J., Losada, I.J., Losada, M.A., 1999. Hydrodynamics induced by wind waves in a vegetation field. J. Geophys. Res. 104, 18383–18396. http://dx.doi.org/10.1029/1999JC900119.

Moeller, I., Spencert, T., French, J.R., 1996. Wind wave attenuation over saltmarsh surfaces: Preliminary results from Norfolk, England. J. Coast. Res. 12, 1009–1016.

Mullarney, J.C., Henderson, S.M., 2010. Wave-forced motion of submerged single-stem vegetation. J. Geophys. Res. 115, C12061. http://dx.doi.org/10.1029/2010/C006448.

Nada, R.M., Khedr, A.H.A., Serag, M.S., El-Nagar, N.A., 2015. Growth, photosynthesis and stress-inducible genes of *Phragmites australis* (Cav.) Trin. ex Steudel from different habitats. Aquat. Bot. 124, 54–62. http://dx.doi.org/10.1016/j.aquabot.2015.03.007.

Nikora, V., Goring, D., 2000. Flow turbulence over fixed and weakly mobile gravel beds. J. Hydraul. Eng. 126, 679–690. http://dx.doi.org/10.1061/(ASCE)0733-9429(2000)126:9(679).

Ostendorp, W., Möller, J., 1991. EM-algorithm as a tool for structure analysis of stands of the common reed (Phragmites australis). Ecol. Model. 53, 27–38. http://dx.doi.org/10.1016/0304-3800(91)90139-R.

Païdoussis, M., Price, S., de Langre, E., 2010. Fluid-Structure Interactions: Cross-Flow-Induced Instabilities. Cambridge University Press, Cambridge, http://dx.doi.org/10.1017/CB09780511760792.

Paquier, A.-E., Meulé, S., Anthony, E.J., Larroudé, P., Bernard, G., 2019. Wind-induced hydrodynamic interactions with aquatic vegetation in a fetch-limited setting: Implications for coastal sedimentation and protection. Estuar. Coasts 42, 688–707. http://dx.doi.org/10.1007/s12237-018-00487-

Paul, M., Bouma, T., Amos, C., 2012. Wave attenuation by submerged vegetation: combining the effect of organism traits and tidal current. Mar. Ecol. Prog. Ser. 444, 31–41. http://dx.doi.org/10.3354/meps09489.

Paul, M., Rupprecht, F., Möller, I., Bouma, T.J., Spencer, T., Kudella, M., Wolters, G., Wesenbeeck, B.K. van, Jensen, K., Miranda-Lange, M., Schimmels, S., 2016. Plant stiffness and biomass as drivers for drag forces under extreme wave loading: A flume study on mimics. Coast. Eng. 117, 70–78. http://dx.doi.org/10.1016/j.coastaleng.2016.07.004.

Py, C., De Langre, E., Moulia, B., 2006. A frequency lock-in mechanism in the interaction between wind and crop canopies. J. Fluid Mech. 568, 425. http://dx.doi.org/10.1017/S0022112006002667.

Ritterbusch, D., 2007. Growth patterns of reed (*Phragmites australis*): the development of reed stands in carp ponds. Aquacult. Int. 15, 191–199. http://dx.doi.org/10.1007/s10499-007-9091-4.

Rupprecht, F., 2015. Vegetation Succession and Coastal Protection by Wave Dissipation in Salt Marshes of North-West Europe. Universität Hamburg. Sarpkaya, T., O'Keefe, J.L., 1996. Oscillating flow about two and three-dimensional bilge keels. J. Offshore Mech. Arct. Eng. 118, 1–6. http://dx.doi.org/10.1115/1.2828796.

Schaefer, R., 2019. Impacts and Vegetation-Induced Attenuation of Wind-and Vessel-Generated Waves. University of Delaware.

Schoutens, K., Heuner, M., Fuchs, E., Minden, V., Schulte-Ostermann, T., Belliard, J.-P., Bouma, T.J., Temmerman, S., 2020. Nature-based shoreline protection by tidal marsh plants depends on trade-offs between avoidance and attenuation of hydrodynamic forces. Estuar. Coast. Shelf Sci. 236, 106645. http://dx.doi.org/10.1016/j.ecss.2020.106645.

Silinski, A., Heuner, M., Schoelynck, J., Puijalon, S., Schröder, U., Fuchs, E., Troch, P., Bouma, T.J., Meire, P., Temmerman, S., 2015. Effects of wind waves versus ship waves on tidal marsh plants: A flume study on different life stages of scirpus maritimus. PLoS ONE 10, e0118687. http://dx.doi.org/10.1371/journal.pone.0118687.

Smith, S.G., Yatskievych, G., 1996. Notes on the genus Scirpus sensu lato in i missouri. Rhodora 98, 168-179.

So, R.M.C., Zhou, Y., Liu, M.H., 2000. Free vibrations of an elastic cylinder in a cross flow and their effects on the near wake. Exp. Fluids 29, 130–144. http://dx.doi.org/10.1007/s003489900065.

Sutton-Grier, A.E., Wowk, K., Bamford, H., 2015. Future of our coasts: The potential for natural and hybrid infrastructure to enhance the resilience of our coastal communities, economies and ecosystems. Environ. Sci. Policy 51, 137–148. http://dx.doi.org/10.1016/j.envsci.2015.04.006.

Västilä, K., Järvelä, J., 2014. Modeling the flow resistance of woody vegetation using physically based properties of the foliage and stem. Water Resour. Res. 50, 229–245. http://dx.doi.org/10.1002/2013WR013819.

Vogel, S., 2007. Living in a physical world XI. To twist or bend when stressed. J. Biosci. 32, 643–655. http://dx.doi.org/10.1007/s12038-007-0064-6. Vuik, V., Jonkman, S.N., Borsje, B.W., Suzuki, T., 2016. Nature-based flood protection: The efficiency of vegetated foreshores for reducing wave loads on coastal dikes. Coast. Eng. 116, 42–56. http://dx.doi.org/10.1016/j.coastaleng.2016.06.001.

Vuik, V., Suh Heo, H.Y., Zhu, Z., Borsje, B.W., Jonkman, S.N., 2018. Stem breakage of salt marsh vegetation under wave forcing: A field and model study. Estuar. Coast. Shelf Sci. 200, 41–58. http://dx.doi.org/10.1016/j.ecss.2017.09.028.

Wang, X.Y., Xie, W.M., Zhang, D., He, Q., 2016. Wave and vegetation effects on flow and suspended sediment characteristics: A flume study. Estuar. Coast. Shelf Sci. 182, 1–11. http://dx.doi.org/10.1016/j.ecss.2016.09.009.

Wayne, C.J., 1976. The effects of sea and marsh grass on wave energy. Coast. Res. Notes 4, 6-8.

Whittaker, P., Wilson, C., Aberle, J., Rauch, H.P., Xavier, P., 2013. A drag force model to incorporate the reconfiguration of full-scale riparian trees under hydrodynamic loading. J. Hydraul. Res. 51, 569–580. http://dx.doi.org/10.1080/00221686.2013.822936.

- Wilson, C.A., Hoyt, J., Schnauder, I., 2008. Impact of foliage on the drag force of vegetation in aquatic flows. J. Hydraul. Eng. 134, 885–891. http://dx.doi.org/10.1061/(ASCE)0733-9429(2008)134:7(885).
- Wilson, C.A.M.E., Xavier, P., Schoneboom, T., Aberle, J., Rauch, H.P., Lammeranner, W., Weissteiner, C., Thomas, H., 2010. The hydrodynamic drag of full scale trees. River Flow 453–460.
- Wu, W., Ozeren, Y., Chen, Q., Jadhav, R., Wren, D., 2016. Laboratory and field investigations of wave attenuation by live marsh vegetation 10.
- Xavier, P., Wilson, C., Aberle, J., Rauch, H.P., Lammeranner, W., Thomas, H., 2010. Drag force of flexible submerged trees. In: Proceedings of the HYDRALAB III Joint User Meeting.
- Xi, M., Kong, F., Li, Y., 2017. Temporal variations in growth and aboveground biomass of *Phragmites australis* and *EVI* analysis in jiaozhou bay coastal salt marshes, China. J. Resour. Ecol. 8, 641–647. http://dx.doi.org/10.5814/j.issn.1674-764x.2017.06.011.
- Yang, S.L., Shi, B.W., Bouma, T.J., Ysebaert, T., Luo, X.X., 2012. Wave attenuation at a salt marsh margin: A case study of an exposed coast on the yangtze estuary. Estuar. Coasts 35, 169–182. http://dx.doi.org/10.1007/s12237-011-9424-4.
- Ysebaert, T., Yang, S.-L., Zhang, L., He, Q., Bouma, T.J., Herman, P.M.J., 2011. Wave attenuation by two contrasting ecosystem engineering salt marsh macrophytes in the intertidal pioneer zone. Wetlands 31, 1043–1054. http://dx.doi.org/10.1007/s13157-011-0240-1.
- Zhang, X., Lin, P., Gong, Z., Li, B., Chen, X., 2020. Wave attenuation by Spartina alterniflora under macro-tidal and storm surge conditions. Wetlands http://dx.doi.org/10.1007/s13157-020-01346-w.
- Zhi, Y., Li, H., An, S., Zhao, L., Zhou, C., Deng, Z., 2007. Inter-specific competition: Spartina alterniflora is replacing Spartina anglica in coastal China. Estuar. Coast. Shelf Sci. 74, 437–448. http://dx.doi.org/10.1016/j.ecss.2007.04.026.